

Journal Pre-proof



Targeting the KRAS Oncogene: Synthesis, Physicochemical and Biological Evaluation of Novel G-Quadruplex DNA Binders

Federica D'Aria Physicochemical Studies; Data curation; Validation; Writing - Original draft preparation ,
Vincenzo Maria D'Amore Computational Studies; Data curation; Validation; Writing- Original draft preparation ,
Francesco Saverio Di Leva Computational studies; Conceptualization; Supervision; Funding acquisition; Writing - r
Jussara Amato Physicochemical Studies; Supervision ,
Marco Caterino Physicochemical Studies ,
Pasquale Russomanno Computational Studies ,
Silvia Salerno Chemical Synthesis ,
Elisabetta Barresi Chemical Synthesis ,
Marinella De Leo Chemical Synthesis ,
Anna Maria Marini Chemical Synthesis ,
Sabrina Taliani Chemical Synthesis; Supervision; Funding acquisition ,
Federico Da Settimo Chemical Synthesis; Supervision ,
Gilmar F. Salgado Writing - reviewing & editing ,
Luca Pompili Biological evaluation ,
Pasquale Zizza Biological evaluation; Data Validation; Writing - Original draft preparation ,
Senji Shirasawa Biological evaluation ,
Ettore Novellino Supervision; Funding acquisition ,
Annamaria Biroccio Biological evaluation; Supervision; Funding acquisition ,
Luciana Marinelli Computational Studies; Conceptualization; Supervision; Funding acquisition ,
Concetta Giancola Physicochemical Studies; Conceptualization; Supervision; Funding acquisition; Writing - review

PII: S0928-0987(20)30126-3
DOI: <https://doi.org/10.1016/j.ejps.2020.105337>
Reference: PHASCI 105337

To appear in: *European Journal of Pharmaceutical Sciences*

Received date: 10 February 2020
Revised date: 30 March 2020
Accepted date: 1 April 2020

Please cite this article as: Federica D'Aria Physicochemical Studies; Data curation; Validation; Writing - Original dra
Vincenzo Maria D'Amore Computational Studies; Data curation; Validation; Writing- Original draft preparation ,
Francesco Saverio Di Leva Computational studies; Conceptualization; Supervision; Funding acquisition; Writing - r
Jussara Amato Physicochemical Studies; Supervision , Marco Caterino Physicochemical Studies ,
Pasquale Russomanno Computational Studies , Silvia Salerno Chemical Synthesis ,
Elisabetta Barresi Chemical Synthesis , Marinella De Leo Chemical Synthesis ,
Anna Maria Marini Chemical Synthesis , Sabrina Taliani Chemical Synthesis; Supervision; Funding acquisition ,
Federico Da Settimo Chemical Synthesis; Supervision , Gilmar F. Salgado Writing - reviewing & editing ,
Luca Pompili Biological evaluation , Pasquale Zizza Biological evaluation; Data Validation; Writing - Original draft p
Senji Shirasawa Biological evaluation , Ettore Novellino Supervision; Funding acquisition ,
Annamaria Biroccio Biological evaluation; Supervision; Funding acquisition , Luciana Marinelli Computational Stud
Concetta Giancola Physicochemical Studies; Conceptualization; Supervision; Funding acquisition; Writing - review
Targeting the KRAS Oncogene: Synthesis, Physicochemical and Biological Evaluation of

This is a PDF file of an article that has undergone enhancements after acceptance, such as the addition of a cover page and metadata, and formatting for readability, but it is not yet the definitive version of record. This version will undergo additional copyediting, typesetting and review before it is published in its final form, but we are providing this version to give early visibility of the article. Please note that, during the production process, errors may be discovered which could affect the content, and all legal disclaimers that apply to the journal pertain.

© 2020 Elsevier B.V. All rights reserved.

Targeting the *KRAS* Oncogene: Synthesis, Physicochemical and Biological Evaluation of Novel G-Quadruplex DNA Binders

Federica D'Aria^{a,‡}, Vincenzo Maria D'Amore^{a,‡}, Francesco Saverio Di Leva^{a,*}, Jussara Amato^a,
Marco Caterino^a, Pasquale Russomanno^a, Silvia Salerno^b, Elisabetta Barresi^b, Marinella De
Leo^b, Anna Maria Marini^b, Sabrina Taliani^b, Federico Da Settimo^b, Gilmar F. Salgado^c, Luca
Pompili^d, Pasquale Zizza^d, Senji Shirasawa^e, Ettore Novellino^a, Annamaria Biroccio^d, Luciana
Marinelli^a, Concetta Giancola^{a,*}

^aDepartment of Pharmacy, University of Naples Federico II, via D. Montesano 49, 80131 Napoli, Italy;

^bDepartment of Pharmacy, University of Pisa, via Bonanno 6, 56126, Pisa, Italy;

^cARNA Laboratory, IECB, University of Bordeaux, Inserm U1212, CNRS UMR 5320, F-33600 Pessac,
France;

^dOncogenomic and Epigenetic Unit, IRCCS – Regina Elena National Cancer Institute, Via Elio Chianesi
53, 00144, Rome, Italy;

^eCentral Research Institute for Advanced Molecular Medicine, Fukuoka University, Fukuoka, Japan.

*Corresponding authors:

E-mail: concetta.giancola@unina.it (C. Giancola), francesco.dileva@unina.it (F.S. Di Leva)

‡These authors contributed equally.

KEYWORDS: DNA G-quadruplex; *KRAS*; Drug Discovery; Cancer; Medicinal Chemistry;
Molecular Modeling; Physicochemical Studies

Abstract

The oncogene *KRAS* is involved in the pathogenesis of many tumors such as pancreatic, lung and colorectal cancers, thereby representing a relevant target for the treatment of these diseases. The *KRAS* P1 promoter contains a nuclease hypersensitive, guanine-rich sequence able to fold into a G-quadruplex motif (G4). The stabilization of this G4 structure by small molecules is emerging as a feasible approach to downregulate *KRAS* expression. Here, a set of novel stabilizing molecules was identified through a virtual screening campaign on the NMR structure of the 22-mer *KRAS* G4. The most promising hits were then submitted to structure-activity relationships studies which allowed improving their binding affinity and selectivity over double helix DNA and different G4 topologies. The best derivative (**19**) underwent fluorescence titration experiments and further computational studies to disclose its binding mechanism to *KRAS* G4. Finally, biological assays showed that this compound is capable to reduce the viability of colorectal cancer cells in which mutated *KRAS* acts as a driver oncogene. Thus, **19** might represent the prototype of a new class of drugs for the treatment of tumors that, expressing mutated forms of *KRAS*, are refractory to current therapeutic regimens.

1. Introduction

1.1 G-quadruplexes. Nowadays it is well known that DNA can form alternative higher-order structures that are believed to play important roles in a number of biological processes and in the progression of several diseases (Bacolla and Wells, 2009; Zhao et al., 2010, Amato et al., 2014b; Balasubramanian et al., 2011). Among non-canonical DNA structures are G-quadruplexes (G4s) which are formed by guanine-rich sequences that assemble into guanine tetrads stabilized by Hoogsteen hydrogen bonds and monovalent cations (Bochman et al., 2012). In the last decades, G4s have drawn growing attention as possible druggable anticancer targets because they are located in key genome regions, including promoters of oncogenes such as *MYC*, *VEGF*, *BCL2*, *KIT*, and *KRAS* (Caterino et al., 2020; Cogoi et al., 2004; Cogoi and Xodo, 2006; Dai et al., 2006a, 2006b; Fernando et al., 2006; Rankin et al., 2005; Siddiqui-Jain et al., 2002; Simonsson et al., 1998; Sun et al., 2005), whose expression can be downregulated by G4-stabilizing small molecules (Balasubramanian et al., 2011).

1.2 KRAS. Remarkably, the *KRAS* gene is overexpressed in about 30% of all human cancers, including pancreatic ductal adenocarcinoma, lung and colorectal cancers (Cogoi et al., 2013; Kang et al., 2017; Miglietta et al., 2017; Stephen et al., 2014). *KRAS* (Gene ID: 3845) maps at 12p12.1 and encodes for a 21 kDa membrane GDP/GTPase (UniProt: P01116) whose on/off state is governed by the GTP/GDP homeostasis. Missense point mutations that shift such balance (most frequently at codon 12 and 13) are responsible for a constitutive activation of *KRAS* and downstream cellular signaling pathways (*e.g.* *RAF*, *MEK*, or *PI3K*) (Cox et al., 2014). A direct targeting of *KRAS* and its downstream effectors at protein level has proved unfruitful since long (Haigis, 2017; Hobbs et al., 2016; McCormick, 2016, 2018). Nevertheless, in recent years specific inhibitors of the constitutively active G12C *KRAS* mutant have been developed,

showing promising therapeutic potential (Janes et al., 2018; Lito et al., 2016; Ostrem et al., 2013; Patricelli et al., 2016).

1.3 *KRAS* G4. The nuclease-hypersensitive element (NHE) within the *KRAS* P1 promoter features a G-rich sequence that folds into a G4 whose stabilization by small molecules offers a convenient alternative to downregulate *KRAS* at gene-level (Cogoi et al., 2008; Cogoi and Xodo, 2016; Hoffman et al., 1990; Jordano and Perucho, 1986). Diverse classes of compounds have been tested to this end, such as porphyrins, acridines, anthraquinones, phenanthrolines, perylenes and quinolines (Alzeer et al., 2009; Boschi et al., 2016; Calabrese et al., 2018; Carvalho et al., 2018; Lavrado et al., 2013, 2015; Monchaud and Teulade-Fichou, 2008; Pattanayak et al., 2018). The majority of these compounds share polycyclic and heteroaromatic moieties that grant decent selectivity over the duplex DNA, mainly due to stronger π - π stacking interactions with the guanine tetrads. However, several of these molecules target a large set of G4s rather than a single one, which may cause off-target effects, and lack basic drug-like properties.

1.4 Targeting *KRAS* G4. In this study, a structure-based virtual screening (VS) was performed on the NMR structure of the *KRAS* P1 promoter G-quadruplex (*KRAS* G4) (Kerkour et al., 2017), with the aim to find novel stabilizers of this DNA motif. The VS selected hits were evaluated by thermal melting experiments, and the most promising compounds were then chosen for likewise lead optimization program. The newly synthesized molecules were again evaluated for their *KRAS* G4 stabilizing properties and then assayed for selectivity toward both diverse G4 topologies and duplex DNA. The best performing derivative underwent further fluorescence assays and molecular dynamics calculations to gain insight into the stoichiometry and binding affinity of its interaction with *KRAS* G4, and to disclose its binding mode to this DNA motif. Also, biological analyses were performed to evaluate the effect of this compound on both the

KRAS gene expression and viability in tumor cells expressing constitutively active forms of mutated *KRAS* (Downward, 2003).

2. Materials and Methods

2.1 Virtual Screening and Molecular Docking. For our study, an in-house virtual database of 5,858 compounds held by the Computational Chemistry Lab of the Department of Pharmacy of the University of Naples Federico II and the commercially available Asinex Platinum Collection library (<http://www.asinex.com>) of 9,216 molecules were selected. Both the selected libraries had been preliminary filtered to include molecules endowed with lead-like pharmacokinetic properties, according to the Lipinski's rule of five. All the possible tautomeric and protonation states in the pH range 7.4 ± 1.5 were generated for each compound using Epik (Greenwood et al., 2010; Shelley et al., 2007) for a total amount of 7,924 and 17,500 structures, respectively, for the in-house and the Asinex libraries. A filtering procedure (see paragraph 3.1 for details) was then applied to retain all the molecules having at least two aromatic rings and a positive total charge, resulting in two final subsets containing, respectively, 875 and 14,280 structures. The NMR structure of the *KRAS* G4 DNA motif (PDB code: 5I2V) (Kerkour et al., 2017) was selected as target macromolecule and prepared through the Protein Preparation Wizard implemented in Maestro Suite 2019 (Madhavi Sastry et al., 2013). During the preparation, all water molecules were deleted, hydrogen atoms were added, and the complex was minimized. The docking search area was set on the center of mass of the macromolecule so as to enclose the entire G4. The interaction grids were thus computed through the grid generation tool of Glide 6.7 (Friesner et al., 2004; Halgren et al., 2004). The OPLS 2005 force field (Banks et al., 2005) was employed for docking. The best 500 initial poses per ligand were retained for post-docking energy

minimization. Otherwise, default parameters were applied. The results from each set of calculations were evaluated and ranked based on the Glide SP scoring function (Friesner et al., 2004; Halgren et al., 2004). For each compound, only the best scored docking pose was retained. The top-ranked molecules (the best 15 %) of each subset were then visually inspected for their binding modes and for good chemical geometry. Compounds **1-4** were retrieved from our in-house library, while compounds **5-12** were purchased from the Asinex vendor. Compounds purity (> 95 %) was determined by HPLC, according to the procedure described in the chemistry section.

2.2 DNA synthesis and sample preparation. The sequences d(AGGGCGGTGTGGGAATAGGGAA) (*KRAS* G4), d(AGGGAGGGCGCTGGGAGGAGGG) (*KIT* G4), d(TAGGGTTAGGGTTAGGGTTAGGG) (Tel23), and d(CGAATTCGTTTTCGAATTCG) (hairpin duplex), were synthesized on a ABI394 DNA/RNA synthesizer (Applied Biosystem, Foster City, CA, USA) by using the standard DNA synthesis protocol on solid phase at the 5- μ mol scale (Oliviero et al., 2010). A concentrated ammonia aqueous solution at 55 °C for 12 h was used to DNA detachment from support and removal of the semi-permanent protection groups. The combined filtrates and washings were concentrated under reduced pressure, dissolved in water, and purified by HPLC on a Nucleogel SAX column (Macherey-Nagel, 1000-8/46), using buffer A consisting of 20 mM KH_2PO_4 / K_2HPO_4 aqueous solution (pH 7.0), containing 20% (v/v) CH_3CN , buffer B consisting of 1 M KCl, 20 mM KH_2PO_4 / K_2HPO_4 aqueous solution (pH 7.0), containing 20% (v/v) CH_3CN , and a linear gradient from 0% to 100% B for 30 min with a flow rate 1 mL min⁻¹. The fractions of the oligomers were collected and successively desalted by Sep-Pak cartridges (C-18).

Oligonucleotide samples were prepared by dissolving the lyophilized DNAs in potassium phosphate buffer (60 mM KCl, 20 mM KH₂PO₄, 0.1 mM EDTA, pH 7.0). The solutions were heated at 90 °C for 5 min and slowly cooled to room temperature. The annealing procedure was followed by overnight storage at 4 °C prior to use. The concentration of the oligonucleotides was evaluated by UV measurements at 260 nm, at a temperature of 90 °C, using molar extinction coefficient values calculated by the nearest-neighbor model (Cantor et al., 1970). Stock solutions of putative ligands were prepared at 10 mM concentration in DMSO. Appropriate amounts of ligand were added to the oligonucleotide solutions to obtain the desired ligand/DNA ratio, followed by mix at 20 °C for 10 min before data acquisition.

2.3 Circular Dichroism. CD spectra were recorded on a Jasco J-815 spectropolarimeter (JASCO Inc., Tokyo, Japan) equipped with a PTC-423S/15 Peltier temperature controller. All the spectra were recorded at 20 °C in the 220-360 nm wavelength range and averaged over three scans. The scan rate was 100 nm min⁻¹, with a 4 s response and 1 nm bandwidth. Buffer baseline was subtracted from each spectrum. Sample concentration was 2 μM for all DNA samples. CD spectra of DNA/ligand mixtures were obtained by adding 10 mol equiv of ligand. CD melting experiments were carried out in the 20-100 °C range at 1 °C min⁻¹ heating rate and followed at an appropriate wavelength for each DNA sample (*KRAS* G4 and *KIT* G4 at 264 nm, Tel23 at 289 nm, and the duplex hairpin at 280 nm). The melting temperatures (T_m) were determined from curve fit using Origin 7.0 software (OriginLab Corp., Northampton, MA, USA). CD melting experiments were recorded on DNA samples both in the absence and presence of each ligand to obtain ΔT_m values, determined as:

$$\Delta T_m = T_{m,DNA/ligand} - T_{m,DNA}$$

where $T_{m,DNA/ligand}$ is measured on ligand/DNA mixtures (10 mol equiv), $T_{m,DNA}$ is from the standalone DNA sample. All experiments were performed in duplicate and the reported values are the average of two measurements.

2.4 Chemistry. The uncorrected melting points were determined using a Reichert Köfler hot-stage apparatus. NMR spectra were obtained on a Bruker AVANCE 400 (1H , 400 MHz, ^{13}C , 100 MHz) in DMSO- d_6 or in $CDCl_3$ (Fig. S1 and S2). The coupling constants are given in Hertz. Magnesium sulfate was used as the drying agent. Evaporations were made in vacuo (rotating evaporator). Analytical TLC have been carried out on Merck 0.2 mm precoated silica gel aluminum sheets (60 F-254). Silica gel 60 (230–400 mesh) was used for column chromatography. ESI-MS/MS were obtained in positive ion mode from an LCQ Advantage ThermoFinnigan spectrometer (ThermoFinnigan, USA). Microwave assisted reactions were carried out in BIOTAGE Initiator 2.5 microwave apparatus. Reagents, starting materials, and solvents were purchased from commercial suppliers and used as received. The following compounds were obtained according to methods previously described: 6-(2-((2-hydroxyethyl)amino)ethyl)benzo[4,5]imidazo[2,1-*b*]quinazolin-12(6*H*)-one (**1**) (Dalla Via et al., 2001), *N*,10-bis(2-(diethylamino)ethyl)-4-oxo-4,10-dihydrobenzo[4,5]imidazo[1,2-*a*]pyrimidine-3-carboxamide (**2**) (Da Settimo et al., 2003), 7-(3-(dimethylamino)propyl)benzo[4,5]imidazo[1,2-*a*]pyrido[3,2-*e*]pyrimidin-5(7*H*)-one (**3**) (Da Settimo et al., 1998), 1,11-dimethyl-5-oxo-5,11-dihydrobenzo[4,5]imidazo[1,2-*a*]pyrido[2,3-*d*]pyrimidin-1-ium iodide (**4**) (Caroti et al., 1987), 1-dialkylaminoalkyl-2-aminobenzimidazoles (**20a-d**) (Dalla Via et al., 2001) and 11-methylbenzo[4,5]imidazo[1,2-*a*]pyrido[2,3-*d*]pyrimidin-5(11*H*)-one (**21**) (Caroti et al., 1987).

Purity of the target compounds was determined using a Shimadzu LC-20AD SP liquid chromatograph equipped with a DDA Detector at 254 nm (column C18 (250 mm x 4.6 mm, 5 μ m, Shim-pack)). The mobile phase, delivered at isocratic flow, consisted of acetonitrile (60%) and phosphate buffered saline (PBS) (40%) and a flow rate of 1.0 mL/min. All the compounds showed percent purity values of $\geq 95\%$.

The structural characterization of previously described target compounds **1-4** and **13-16** has been herein implemented by ^{13}C NMR data.

6-(2-((2-Hydroxyethyl)amino)ethyl)benzo[4,5]imidazo[2,1-b]quinazolin-12(6H)-one (**1**). ^{13}C NMR (100 MHz, DMSO- d_6): δ 42.27, 47.17, 51.77, 60.78, 109.94, 115.53, 116.60, 122.03, 122.97, 125.63, 125.93, 126.42, 126.84, 132.53, 134.82, 146.87, 149.48, 159.61.

N,10-Bis(2-(diethylamino)ethyl)-4-oxo-4,10-dihydrobenzo[4,5]imidazo[1,2-a]pyrimidine-3-carboxamide (**2**). ^{13}C NMR (100 MHz, CDCl $_3$): δ 12.07, 12.30, 37.62, 41.93, 47.59, 47.64, 50.90, 52.08, 107.16, 110.11, 117.73, 123.80, 125.95, 127.10, 131.54, 149.75, 159.34, 160.27, 164.85.

7-(3-(Dimethylamino)propyl)benzo[4,5]imidazo[1,2-a]pyrido[3,2-e]pyrimidin-5(7H)-one (**3**). ^{13}C NMR (100 MHz, CDCl $_3$): δ 26.29, 40.57, 45.51, 56.43, 110.08, 114.96, 116.30, 122.20, 123.86, 125.64, 126.49, 131.49, 138.65, 149.20, 151.00, 152.71, 168.85.

1,11-Dimethyl-5-oxo-5,11-dihydrobenzo[4,5]imidazo[1,2-a]pyrido[2,3-d]pyrimidin-1-ium iodide (**4**). ^{13}C NMR (100 MHz, DMSO- d_6): δ 29.14, 42.02, 111.34, 115.39, 116.96, 124.60, 124.81, 127.30, 131.50, 144.78, 148.79, 150.44, 152.52, 156.86.

General procedure for the synthesis of 6-(aminoalkyl)benzo[4,5]imidazo[2,1-b]quinazolin-12(6H)-one derivatives 13-16. A mixture of the appropriate 1-dialkylaminoalkyl-2-aminobenzimidazole **20a-d** (0.50 mmol), 2-chlorobenzoic acid (0.078 g, 0.50 mmol), cuprous bromide (0.004 g, 0.030 mmol), anhydrous potassium carbonate (0.083 g, 0.60 mmol) and a

catalytic amount of potassium iodide in 1.0 mL of dimethylformamide was irradiated at a T = 150 °C, P = 10 bar, power = 40-150 Watt, *ramp* time = 2 min for 12 min. After cooling the reaction mixture was poured into ice. The precipitated crude products **13-16** were collected and purified by recrystallization from ethanol.

6-(2-(Dimethylamino)ethyl)benzo[4,5]imidazo[2,1-b]quinazolin-12(6H)-one (13). Yield: 70%; m.p. 161-162 °C (lit. ref. 43, m.p. 160-165 °C); ¹³C NMR (100 MHz, CDCl₃): δ 40.44, 45.88, 56.75, 108.51, 116.62, 117.12, 122.37, 123.17, 126.02, 126.20, 126.35, 127.26, 131.99, 134.59, 146.69, 149.55, 160.31.

6-(2-(Diethylamino)ethyl)benzo[4,5]imidazo[2,1-b]quinazolin-12(6H)-one (14). Yield: 65%; m.p. 143-144 °C (lit. ref. 43, m.p. 140-145 °C); ¹³C NMR (100 MHz, CDCl₃): δ 11.49, 40.13, 47.70, 50.07, 108.78, 116.60, 117.16, 122.47, 123.26, 126.00, 126.16, 126.47, 127.33, 131.99, 134.65, 146.68, 149.53, 160.32.

6-(3-(Dimethylamino)propyl)benzo[4,5]imidazo[2,1-b]quinazolin-12(6H)-one (15). Yield: 55%; m. p. 163-164 °C (lit. ref. 43, m.p. 163-165 °C); ¹³C NMR (100 MHz, CDCl₃): δ 25.85, 40.31, 45.25, 56.51, 108.55, 116.61, 117.10, 122.39, 123.21, 126.01, 126.12, 126.42, 127.30, 132.15, 134.66, 146.74, 149.60, 160.34.

6-(3-(Diethylamino)propyl)benzo[4,5]imidazo[2,1-b]quinazolin-12(6H)-one (16). Yield: 65%; m.p. 131-133 °C (lit. ref. 43, m.p. 130-135 °C); ¹³C NMR (100 MHz, CDCl₃): δ 10.64, 24.99, 40.57, 46.96, 50.27, 108.59, 116.66, 117.14, 122.53, 123.29, 125.93, 126.14, 126.52, 127.35, 131.93, 134.71, 146.77, 149.52, 160.30.

General synthetic procedures for 3-(2-substituted-ethyl)-12-methyl-6-oxo-2,3,6,12-tetrahydro-1H-benzo[4,5]imidazo[1,2-a]imidazo[1',2':1,6]pyrido[2,3-d]pyrimidin-14-ium bromide 17-19. The appropriate amine (10.0 mmol) was added dropwise to a suspension of **22**

(0.110 g, 0.25 mmol) in 10 ml of ethanol and the mixture was refluxed for 4 h. After cooling, the resulting suspension was filtered, and the crude products obtained were purified by recrystallization from ethanol.

3-(2-Hydroxyethyl)-12-methyl-6-oxo-2,3,6,12-tetrahydro-1H-benzo[4,5]imidazo[1,2-a]imidazo[1',2':1,6]pyrido[2,3-d]pyrimidin-14-ium bromide (17). Yield: 45%; ^1H NMR (400 MHz, DMSO- d_6): δ 3.71 (s, 4H), 3.87 (s, 3H), 4.20 (t, $J = 10.0$ Hz, 2H), 4.65 (t, $J = 10.0$ Hz, 2H), 5.07 (s, 1H), 6.95 (d, $J = 9.2$ Hz, 1H), 7.53 (t, $J = 7.4$ Hz, 1H), 7.65 (t, $J = 7.6$ Hz, 1H), 7.83 (d, $J = 8.0$ Hz, 1H), 8.47-8.51 (m, 2H); ^{13}C NMR (100 MHz, DMSO- d_6): δ 28.90, 45.40, 48.39, 48.60, 57.74, 100.68, 100.81, 110.96, 115.36, 123.97, 125.22, 126.64, 131.48, 141.79, 148.96, 151.43, 156.47, 156.61. ESI-MS/MS m/z 336 $[\text{M}]^+$. Anal. Calcd. for $\text{C}_{18}\text{H}_{18}\text{BrN}_5\text{O}_2$ (%): C, 51.94; H, 4.36; N, 16.82. Found: C, 52.01; H, 4.29; N, 16.75.

3-(2-(Dimethylamino)ethyl)-12-methyl-6-oxo-2,3,6,12-tetrahydro-1H-benzo[4,5]imidazo[1,2-a]imidazo[1',2':1,6]pyrido[2,3-d]pyrimidin-14-ium bromide (18). Yield: 49%; ^1H NMR (400 MHz, DMSO- d_6): δ 2.23 (s, 6H), 2.56 (t, $J = 6.0$ Hz, 2H), 3.74 (t, $J = 6.0$ Hz, 2H), 3.86 (s, 3H), 4.19 (t, $J = 9.8$ Hz, 2H), 4.64 (t, $J = 10$ Hz, 2H), 7.00 (d, $J = 9.2$ Hz, 1H), 7.52 (t, $J = 7.2$ Hz, 1H), 7.64 (t, $J = 7.2$ Hz, 1H), 7.82 (d, $J = 8.0$ Hz, 1H), 8.45-8.50 (m, 2H); ^{13}C NMR (100 MHz, DMSO- d_6): δ 28.78, 43.44, 45.22, 48.26, 55.62, 100.14, 100.80, 110.84, 115.21, 123.86, 125.03, 126.53, 131.31, 141.85, 148.76, 151.34, 156.06, 156.28. ESI-MS/MS m/z 363 $[\text{M}]^+$. Anal. Calcd. for $\text{C}_{20}\text{H}_{23}\text{BrN}_6\text{O}$ (%): C, 54.18; H, 5.23; N, 18.96. Found: C, 54.32; H, 5.19; N, 18.81.

3-(2-(Diethylamino)ethyl)-12-methyl-6-oxo-2,3,6,12-tetrahydro-1H-benzo[4,5]imidazo[1,2-a]imidazo[1',2':1,6]pyrido[2,3-d]pyrimidin-14-ium bromide (19). Yield: 50%; ^1H NMR (400 MHz, DMSO- d_6): δ 0.93 (t, $J = 7.0$ Hz, 6H), 2.53 (q, $J = 7.2$ Hz, 4H), 2.68 (t, $J = 5.6$ Hz, 2H), 3.70 (t, $J = 5.8$ Hz, 2H), 3.86 (s, 3H), 4.21 (t, $J = 10$ Hz, 2H), 4.66 (t, $J = 9.8$ Hz, 2H), 6.96 (d, J

= 9.2 Hz, 1H), 7.52 (t, $J = 7.6$ Hz, 1H), 7.64 (t, $J = 7.8$ Hz, 1H), 7.82 (d, $J = 8.0$ Hz, 1H), 8.45-8.50 (m, 2H); ^{13}C NMR (100 MHz, DMSO- d_6): δ 11.79, 28.90, 44.12, 45.33, 46.30, 48.54, 49.65, 100.54, 100.85, 110.97, 115.34, 123.97, 125.17, 126.63, 131.44, 141.72, 148.91, 151.45, 156.21, 156.45. ESI-MS/MS m/z 391 $[\text{M}]^+$. Anal. Calcd. for $\text{C}_{22}\text{H}_{27}\text{BrN}_6\text{O}$ (%): C, 56.05; H, 5.77; N, 17.83. Found: C, 56.21; H, 5.71; N, 17.68.

1-(2-Bromoethyl)-11-methyl-5-oxo-5,11-dihydrobenzo[4,5]imidazo[1,2-*a*]pyrido[2,3-*d*]pyrimidin-1-ium bromide 22. Compound **21** (0.215 g, 0.86 mmol) was suspended in 1.5 mL of 1,2-dibromoethane (17.0 mmol). The resulting mixture was heated at 90 °C for 40 h. During this time an additional amount of 1,2-dibromoethane (0.2 ml) was slowly added. After cooling, the suspension was filtered to give a yellow solid, which was purified by recrystallization from ethanol. Yield: 65%; ^1H NMR (400 MHz, DMSO- d_6): δ 3.97 (s, 3H), 4.17 (t, $J = 6.0$ Hz, 2H), 5.25 (t, $J = 6.0$ Hz, 2H), 7.63 (t, $J = 6.8$ Hz, 1H), 7.72 (t, $J = 7.0$ Hz, 1H), 7.76-7.79 (m, 1H), 7.91 (d, $J = 8.0$ Hz, 1H), 8.49 (d, $J = 8.0$ Hz, 1H), 9.20 (d, $J = 6.0$ Hz, 1H), 9.26 (dd, $J = 1.8$ Hz, $J = 7.8$ Hz, 1H).

2.5 Fluorescence. Fluorescence experiments were performed at 20 °C on an FP-8300 spectrofluorimeter (Jasco Inc., Tokyo, Japan) equipped with a Peltier temperature controller accessory (Jasco PCT-818). A 1 cm path length, sealed quartz cuvette was used. Both excitation and emission slits were set at 5 nm. The ligand solutions had a concentration in the 1.5-2.0 μM range in phosphate buffer and were prepared by weighting using an analytical scale. The titrations were carried out by stepwise additions of DNA (5 μL at 100 μM) to a cell containing a fixed concentration (1.5-2.0 μM) of ligand. The solution was stirred and allowed to equilibrate for 5 min after each addition. Emission spectra were recorded by exciting each compound at the

appropriate wavelength. The fraction of bound ligand (α) at each point of the titration was calculated following fluorescence changes at the maximum of intensity:

$$\alpha = \frac{I_{\lambda} - I_{\lambda}^{max}}{I_{\lambda}^{min} - I_{\lambda}^{max}}$$

in which λ is the wavelength of the ligand maximum emission; I_{λ} is the fluorescence intensity at each point of titration; I_{λ}^{max} is the fluorescence intensity of the ligand alone; and I_{λ}^{min} is the fluorescence intensity of the saturated sample.

Titration curves were obtained by plotting α versus the DNA G4 concentration. The equilibrium binding constant (K_b) and the stoichiometry of the binding (n) were estimated by fitting the resulting curve to an independent and equivalent binding site model (Cummaro et al., 2011):

$$\alpha = (1/2 L_0) \left[(L_0 + nQ_0 + 1/K_b) - \sqrt{(L_0 + nQ_0 + 1/K_b)^2 - 4L_0nQ_0} \right]$$

in which α is the bound ligand fraction, L_0 is the total ligand concentration, and Q_0 is the added G4 concentration. Appropriate excitation wavelength was use for each ligand. Experiments were repeated twice and the results are reported as the mean \pm S.D..

2.6 Native polyacrylamide gel electrophoresis (PAGE) analysis. Native gel electrophoreses were carried out in 15% (w/v) polyacrylamide gel. An 89 mM Tris HCl, 89 mM boric acid 10 \times TB solution at pH 7.0 was used as a run buffer, APS as a radical initiator, TEMED as a radical stabilizer and bromophenol blue as a run marker. Stock ligand solutions concentration was 10 mM in DMSO. Two native gel electrophoreses were carried out in excess of either the ligand or the oligonucleotide. In the first case, an oligonucleotide concentration of 50 μ M for each sample and an increasing amount (1, 2, 10 mol equiv) of ligand were used. In the second case, an oligonucleotide concentration of 50 μ M for each sample and an increasing amount (0.01, 0.02,

0.1 mol equiv) of ligand were used. The total volume loaded in each well was 10 μ L. Gels were imaged by UV-shadowing, using 254 nm exposure wavelength (Amato et al., 2014a).

2.7 Molecular Dynamics. Docking simulations on compound **19** were performed applying the same protocol followed in VS calculations. Prior to docking, the ligand tridimensional structure was generated with the Maestro Build Panel, and its tautomeric and protonation states at physiological pH (7.4 ± 1.5) were then predicted by Epik (Greenwood et al., 2010; Shelley et al., 2007). The docking predicted **19**/*KRAS* G4 complexes were solvated in a 12.0 Å layer cubic water box using the TIP3P water model parameters (Jorgensen et al., 1983). 19 K^+ cations were used to neutralize each system, with two of these ions placed at the center of the G-tetrads. Further 2 K^+ and 2 Cl^- ions were added to reach the standard 150 mM KCl concentration. The *parmbsc1* (Ivani et al., 2015) and *gaff* (Wang et al., 2004) Amber force fields were used to parameterize the nucleic acid and ligand, respectively. Amber charges were applied to the DNA and water molecules, whereas ligand charges were computed using the restrained electrostatic potential (RESP) fitting procedure (Bayly et al., 1993). The ESP was first calculated by means of the Gaussian package (Frisch et al., 2009) using a 6-31G* basis set at B3LYP level of theory, and then the RESP charges (Wang et al., 2000) were obtained by a two-stages fitting procedure using Antechamber (Wang et al., 2006). The NAMD 2.13 (Phillips et al., 2005) code was used to perform the simulations. A cutoff of 10 Å was used for short-range interactions. The long-range electrostatic interactions were computed by means of the particle mesh Ewald method (Darden et al., 1993) using a 1.0 Å grid spacing in periodic boundary conditions. The SHAKE algorithm (Ryckaert et al., 1977) was applied to constraint bonds involving hydrogen atoms and the non-iterative SETTLE method (Miyamoto and Kollman, 1992) to keep waters rigid, which allowed a

2 fs integration time step. A conjugate gradient energy minimization of 10,000 steps was performed on each system in two stages. In the first step, the system heavy atoms were kept fixed in order to relax only the hydrogens and the water molecules, while during the second step all the atomic positions were minimized. Then, each complex was heated up to 300 K using the Langevin thermostat (Grest and Kremer, 1986) in three stages of 250 ps each, and then pressurized to 1 atm for 250 ps using the Langevin piston Nose-Hoover method implemented in NAMD (Feller et al., 1995; Martyna et al., 1994). During the equilibration process harmonic constraints were put on both the ligand and DNA heavy atoms, which were gradually released along the process. The production runs were performed in the NPT ensemble at 1 atm and 300 K. The stability of each docking-predicted pose of **19** along MD simulations was evaluated through RMSD calculations on the heavy atoms of the ligand polycyclic scaffold. The effects of the ligand binding on the overall architecture of *KRAS* G4 were measured through the RMSD plots of the DNA backbone heavy atoms. Prior to each RMSD calculation, trajectory frames were aligned on the DNA guanine residues heavy atoms.

2.8 Cell lines, culture conditions and treatments. HCT116 colorectal cancer cells were obtained by Dr Vogelstein, Johns Hopkins University. HK2-6 and HKE-3 were kindly provided by Dr. Shirasawa and performed by gene targeting technique (Shirasawa et al., 1993). BJ-EHLT derived from the transformation of BJ human fibroblasts with hTERT and SV40 early region. All the cells were grown in high glucose Dulbecco modified eagle medium (DMEM; Euroclone) supplemented with L-glutamine, penicillin/streptomycin and 10% fetal bovine serum (FBS, Hyclone). The G-quadruplex ligand EMICORON (Franceschin et al., 2012; Zizza et al., 2019) was used at 1 μ M for 24 h.

2.9 Real-time PCR. To quantify gene expression by real-time quantitative polymerase chain reaction (qRT-PCR), total RNA was isolated from cell pellets by using TRIzol reagent (Ambion). The quality of the extracted RNA was assessed by 1% agarose gel electrophoresis and from the A_{260}/A_{280} absorbance ratio (Nanodrop 1000, ThermoFisher Scientific). Reverse transcription (RT) from 500 ng of RNA was performed using the QuantiTect Reverse Transcription Kit (Qiagen) according to the manufacturer's instructions. Real-time qRT-PCRs were performed on the obtained cDNAs by using Fast power SYBR green master mix (Apply Biosystem) on 7900HT Fast Real-Time PCR System (Applied Biosystem) thermocycler. For each sample 5 μ l of the 1:10 diluted cDNA was mixed with 0.5 μ l of each primer (10 μ M), 10 μ l of the SYBR green master mix and water at final volume of 20 μ l. Standard qPCR thermal parameters were used: one cycle of 95 °C for 10 min then 40 cycles at 95 °C for 15 sec and 60 °C for 1 min followed by dissociation curve (95 °C for 15 sec, 60 °C for 1 min, 95 °C for 15 sec).

Primer pairs (KRAS: FW 5'-ACACAAAACAGGCTCAGGACT-3'; REV: 5'-TGTCGGATCTCCCTCACCAA-3' and β -actin: FW 5'-AGCACTGTGTTGGCGTACAG-3'; REV: 5'-TCCCTGGAGAAGAGCTACGA-3') were synthesized by Integrated DNA Technologies (BVBA Leuven, Belgium).

All experiments were run in triplicate and the gene expression levels were normalized to the β -actin.

2.10 Western Blotting. For western blot analysis total cell lysates were prepared as previously reported (Biroccio et al., 2003). The proteins were fractionated by SDS-polyacrylamide gel electrophoresis and transferred to nitrocellulose membrane (Amersham, Arlington Heights,

USA). Membranes were probed with primary antibodies and the signal was detected using peroxidase-conjugated anti-mouse or anti-rabbit secondary antibodies (Jackson ImmunoResearch Labs, Inc., Baltimore, USA). The enhanced chemi-luminescence (ECL) system (Thermo Scientific) was used for detection. The following primary antibodies were used: rabbit mAb anti-RAS (D2C1, Cell Signaling Technology Beverly, MA, USA) (Naidu et al., 2017), mouse mAb anti- β -actin (clone AC-15, Sigma, St. Louis, USA) and mouse mAb anti- γ H2AX (Millipore, Billerica, MA, USA).

2.11 Clonogenic assay. HCT116 cells, were seeded in 35 mm-Petri dishes at the clonogenic density of 300 cells/plate in DMEM medium with 10% FBS and, after 24 h, cells were treated with DMSO (negative control) or the indicated dose of **19**. After 10 days, the cells were stained with 2% methylene blue in 50% ethanol and the number of colonies was counted. Surviving fractions were calculated as the ratio of absolute survival of the treated sample/absolute survival of the untreated sample.

2.12 Viability Assay (Crystal Violet). HK2-6 and HKE-3 cells were seeded in a 24-well plate at a density of 7×10^4 for well. After 24 h, the cells were treated with compound **19** at different doses for 72 h. Then cells were washed twice in PBS and fixed with 4% formaldehyde for 15 min at RT. After washing, 500 μ l of crystal violet staining solution (Sigma) was added to each well, and incubated for 30 min at RT. Finally, the plates were rinsed twice with water, air-dried at RT, and the cell pellets were dissolved in 400 μ l of acetic acid. One hundred μ l of each sample were transferred to a 96-well plate and the optical density of each well was measured at 570 nm (OD570) with an ELISA reader (Thermo Scientific). The average absorbance in each condition was used to calculate the survival expressed as percent of treated vs untreated condition. IC_{50} (the dose necessary to reduce the survival of 50%) was calculated by Calcsyn software.

2.13 Immunofluorescence Microscopy. BJ-EHLT cells were fixed in 2% formaldehyde in phosphate buffered saline (PBS) for 10 min at room temperature and permeabilized in 0.25% Triton X-100 in PBS for 5 min at RT. For immune-labeling, cells were incubated with the mouse anti- γ H2AX (Millipore, Billerica, MA, USA) primary antibody 2h at RT, washed twice in PBS and finally incubated with the anti-mouse IgG (H+L), F(ab')₂ Fragment (Alexa Fluor 555 Conjugate) secondary antibodies for 1 h. Nuclei were stained with 4',6-diamidino-2-phenylindole (DAPI, Sigma). Fluorescence signals were recorded by using a Leica DMIRE2 microscope equipped with a Leica DFC 350FX camera and elaborated by Leica FW4000 deconvolution software (Leica, Solms, Germany). For quantitative analysis of γ H2AX positivity, at least 250 cells on triplicate slices were scored.

3. Results and Discussion

3.1 Virtual Screening. As briefly reported in the introduction, the solved *KRAS* G4 NMR structure (PDB code: 5I2V) (Kerkour et al., 2017) was here used as target for a structure-based virtual screening (VS) campaign aimed at identifying brand new *KRAS* G4 stabilizers. Indeed, this G4 motif possesses two wide stacking surfaces and four grooves of medium size that can potentially be recognized by small organic molecules (Kerkour et al., 2017). For VS calculations, we docked molecules from both the commercial Asinex Platinum Collection library and an in-house database. Notably, the latter library is composed of all the compounds designed, synthesized and tested so far by our research group against common anticancer targets including kinases, integrins, chemokine receptors and nucleic acids. Advantageously, these compounds are either already available in stock or can be easily resynthesized. Moreover, for many molecules, a number of analogues are already present allowing a rapid structure-activity relationship analysis.

Both the selected libraries were prepared as described in Materials and Methods. Then, since the use of appropriate molecular filtering procedures have largely proved to improve the VS success rate (Da Costa et al., 2019; La Pietra et al., 2018; Pinto et al., 2019), all the neutral and negatively charged compounds as well as all the molecules featuring less than two aromatic rings were discarded from both the datasets. In fact, positively charged moieties and extended aromatic systems are generally required to establish favorable contacts with the DNA phosphate backbone and with the G-tetrads stacking surfaces or possibly the G4 grooves, respectively (Castillo-González et al., 2015; Di Leva et al., 2014, 2013). The final subsets from both the libraries were then submitted to VS calculations.

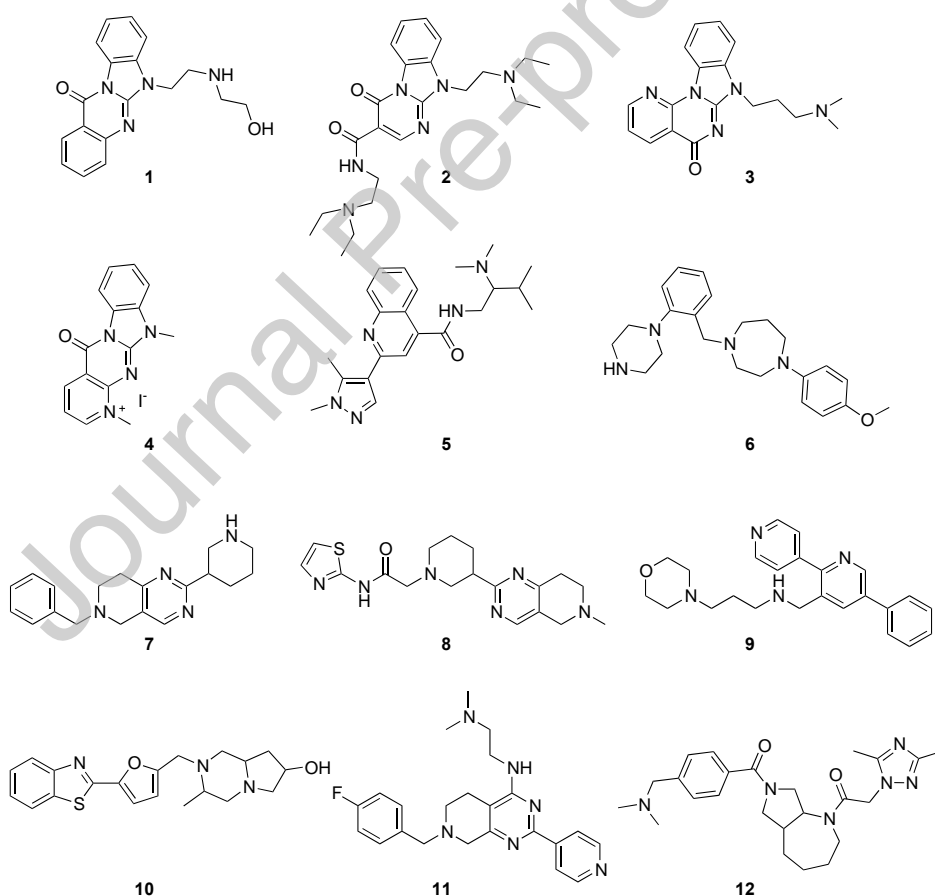


Chart 1. Chemical structures of VS hits **1-4** from the in-house library and **5-12** from the Asinex Platinum Collection.

The top 15% of the ranked solutions from each database was selected to obtain a subset of molecules, all showing a docking score < -7.0 , feasible for the following visual examination. In fact, these compounds were subjected to a careful visual inspection in order to evaluate their predicted interaction mode with *KRAS* G4. In particular, the formation of π -stacking or polar interactions (i.e. salt bridges) with the target DNA was investigated. Finally, the selected compounds were further inspected for good chemical binding geometry. Based on these criteria we chose 12 compounds (Chart 1 and Table S1): 4 were picked from the in-house database (**1-4**), while 8 were taken from the Asinex Platinum Collection library and then purchased from the vendor (**5-12**). Interestingly, the predicted binding modes of the best ranked compounds from each library, namely **1** and **9**, suggested that the chosen molecules could in principle occupy either the G4 stacking surface (Fig. S3A) or the DNA grooves (Fig. S3B). All the compounds were then tested in biophysical assays to verify their G4 binding properties.

3.2 CD Experiments of the selected hits (1-12) with *KRAS* G4. Initially, the conformation of *KRAS* G4 was proved by circular dichroism (CD) spectroscopy. The CD spectrum displayed a positive band at 264 nm and a negative band at 240 nm, which is the characteristic CD profile of parallel-stranded quadruplexes (Zhang et al., 2010). Notably, no CD spectra change has to be reported for *KRAS* G4 upon ligand binding (Fig. S4). The stabilizing effect of each of the selected hits (**1-12**) on *KRAS* G4 was then measured in terms of ΔT_m by CD thermal melting experiments at 264 nm (Fig. 1 and Fig. S5). Compounds **1** and **4** proved the best, albeit not fully satisfactory, stabilizing effect on *KRAS* G4 ($\Delta T_m = +4.5$ °C and $\Delta T_m = +7.5$ °C, respectively; Fig. 2). Thus, the selectivity of these compounds against the 20-mer hairpin DNA was then assessed through CD thermal melting experiments at 280 nm (Fig. S6). These assays showed no

stabilizing effects for **1** and **4** on the duplex DNA, thus prompting their selection as hit compounds for chemical optimization.

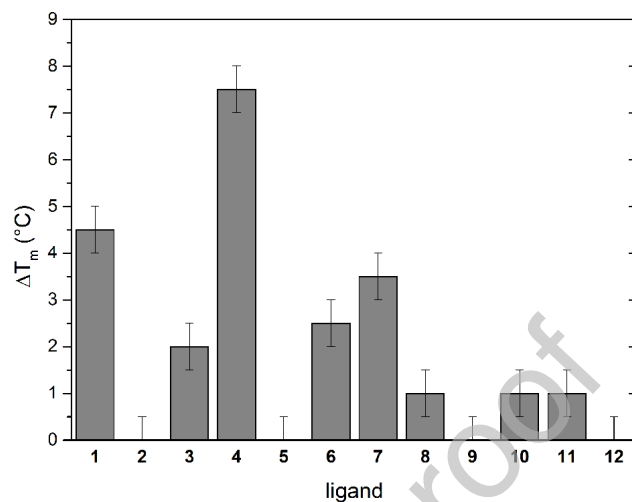


Fig. 1. ΔT_m of KRAS G4 upon interaction with VS hits.

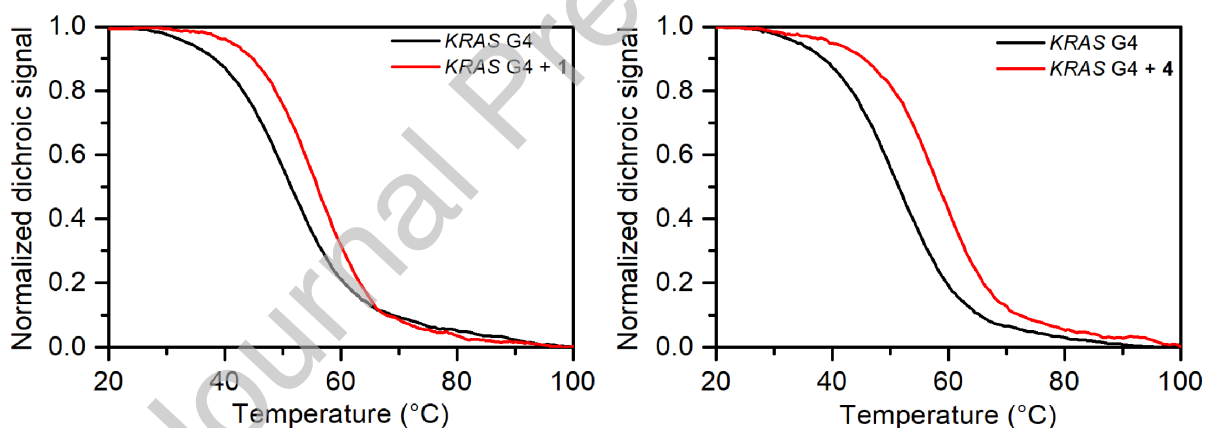


Fig. 2. Normalized CD thermal denaturation of KRAS G4 in the absence and in the presence of **1** (left panel) and **4** (right panel).

3.3 Hit Optimization. In our lead optimization program, we intended to investigate the influence of side chains of different length and nature on the binding of **1** and **4** to the target DNA as well as on their G4/duplex selectivity. In this perspective, we first selected from our in-house database a set of four analogues of **1** (compounds **13-16**, Chart 2), featuring a terminal amino group in

place of the hydroxyl function. In fact, as briefly reported in the introduction, our in-house library offers the advantage that many compounds already possess a number of analogues, so a rapid SAR analysis is possible.

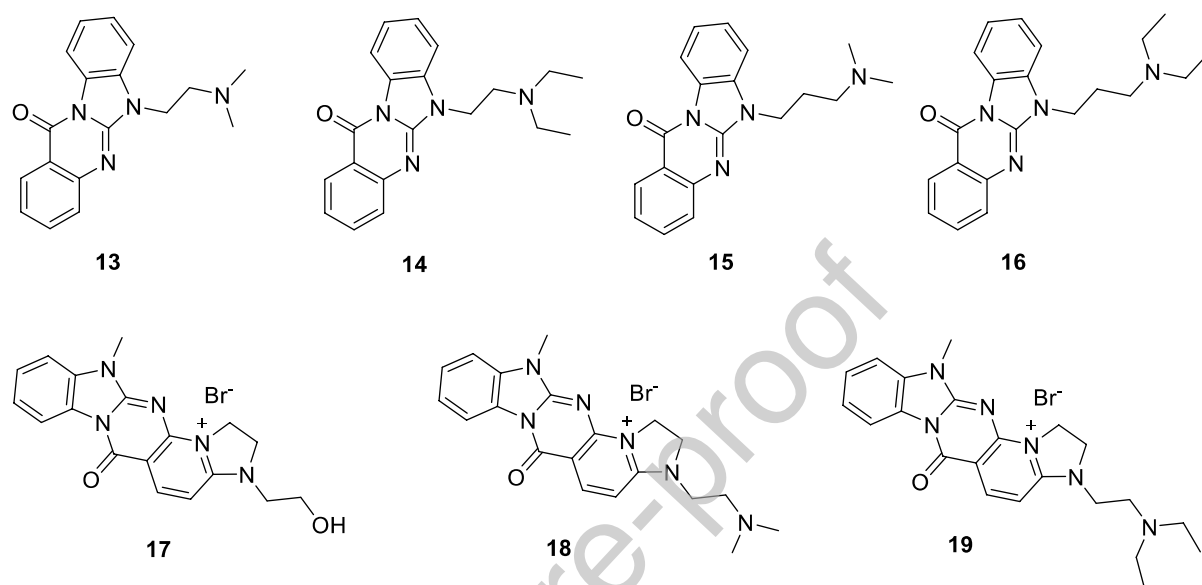
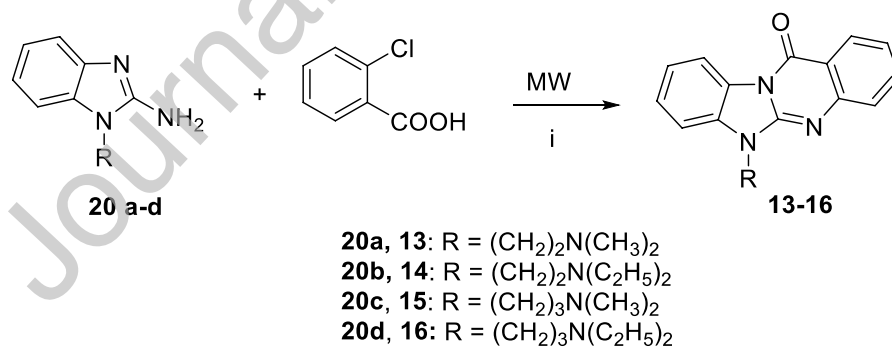


Chart 2. Chemical structures derivatives **13-19**.

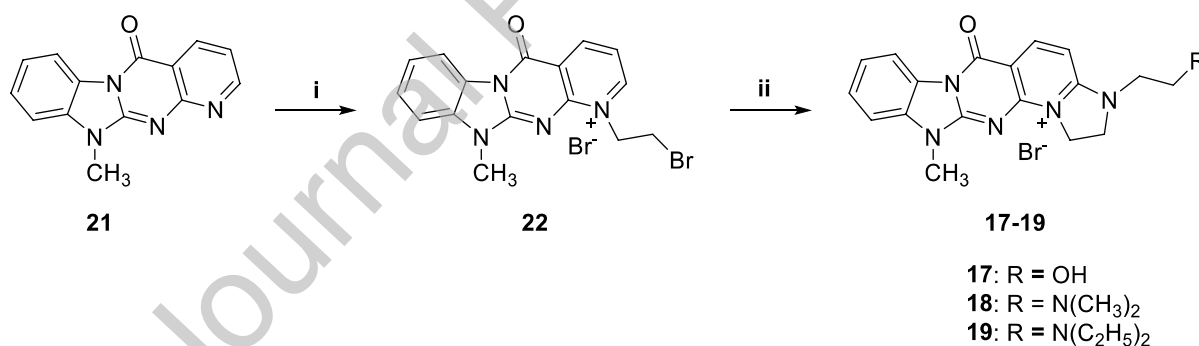


Scheme 1. Synthesis of compounds **13-16**. Reagents and conditions: (i) K₂CO₃, CuBr, KI, DMF, 150 °C, P = 10 bar, power = 40-150 W, ramp t = 2 min, t = 12 min.

However, the synthesis of **13-16** (Dalla Via et al., 2001) has been here improved using microwaves (MW), with higher yields and shorter reaction time (12 min *versus* 5-7 h, Scheme

1). In particular, a MW-assisted Ullmann condensation reaction between the appropriate 1-dialkylaminoalkyl-2-aminobenzimidazole **20a-d** (Dalla Via et al., 2001) and the commercially available 2-chlorobenzoic acid (Scheme 1) was performed. After cooling, the reaction mixture was poured into ice and the precipitated crude 6-(aminoalkyl)benzo[4,5]imidazo[2,1-*b*]quinazolin-12(6*H*)-ones **13-16** were collected and purified by recrystallization from ethanol.

In the case of **4**, we decided to introduce differently functionalized protonable pendant side chains at the positively charged pyridine nitrogen since positively charged moieties are recognized to establish favourable contacts with the phosphate backbone of DNA (Di Leva et al., 2014, 2013). In this vein, the synthetic procedure previously developed by us for the preparation of **4** (Caroti et al., 1987) was applied starting from the 11-methylbenzo[4,5]imidazo[1,2-*a*]pyrido[2,3-*d*]pyrimidin-5(11*H*)-one **21** (Caroti et al., 1987), with few modifications (Scheme 2).



Scheme 2. Synthesis of compounds **17-19**. Reagents and conditions: (i) 1,2-dibromoethane, 90 °C; (ii) H₂N(CH₂)₂R, ethanol, reflux.

Reaction of compound **21** with an excess of 1,2-dibromoethane at 90 °C for 40 h furnished **22**, which was suspended in ethanol and added with an excess of the appropriate amine. The reaction mixture was refluxed for 4 h and then filtered to give crude products, finally purified by recrystallization from ethanol. A deep analysis of the spectral data allowed us to unequivocally

assign to the obtained compounds **17-19** the structures outlined in Scheme 2, featuring a fused pentacyclic system. Actually, this is in agreement with literature data (Parenty et al., 2007, 2005) that report the reaction between a primary amine and a 2-bromoethylpyridinium derivative to proceed via a nucleophilic attack, followed by a cyclisation and an oxidation step, leading to a dihydroimidazopyridinium compound. Although the obtained derivatives **17-19** possessed a rather unexpected structure, they were considered for biological evaluation, as their structural features still met the requirements to act as G4 stabilizing molecules, that is a positively charged pendant chain and an extended aromatic system.

3.4 Biophysical assays on 13-19. Compounds **13-19** were tested on *KRAS* G4 and duplex hairpin DNA, evaluating ΔT_m by CD thermal melting experiments (Fig. 3, 4 and S7-S10). In the subset of derivatives **13-16**, all the compounds except for **13** showed improved *KRAS* G4 stabilizing properties compared to the hit **1** and maintained satisfactory selectivity over duplex hairpin (Fig. 3).

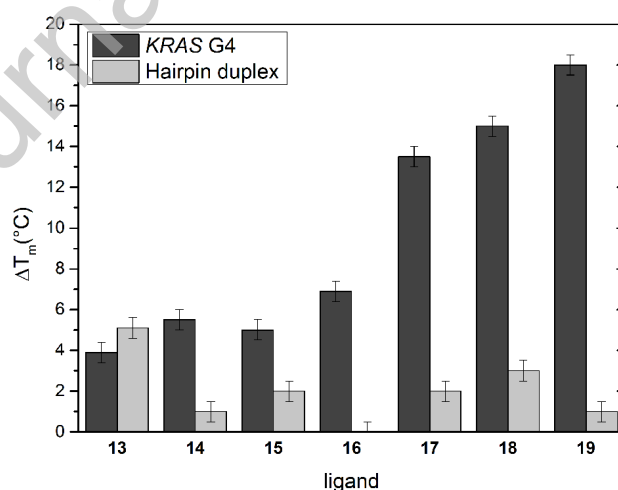


Fig. 3. Ligand-induced thermal stabilization of *KRAS* G4 and hairpin duplex measured by CD melting experiments.

As shown in Fig. 3, the most interesting results were observed for the pentacyclic derivatives **17-19**, with all the three compounds recording substantial performance improvement ($\Delta T_m > 10$ °C) with respect to the parent hit **4** (Fig. 1, $\Delta T_m = 7.5$ °C). Also, these compounds showed high *KRAS* G4/duplex DNA selectivity ratio (Fig. 3). In view of these data, **17-19** were further tested against the parallel *KIT* G4 and hybrid-1 Tel23 (Fig. S11 and S12).

Table 1. Comparison of **17**, **18** and **19** ΔT_m with *KRAS* G4 and control sequences.

ligand	<i>KRAS</i> G4 $\Delta T_m \pm 0.5$ °C	<i>KIT</i> G4 $\Delta T_m \pm 0.5$ °C	Tel23 $\Delta T_m \pm 0.5$ °C
17	+ 13.5	+ 7.0	+ 2.5
18	+ 15.0	+ 10.0	+ 5.5
19	+ 18.0	+ 10.5	+ 7.5

These ligands showed preferential binding to the parallel G4s (Table 1). Indeed, all of them turned out to increase the *KRAS* G4 thermal stability to a larger extent than the other G4s. In particular, **19** was the most potent *KRAS* G4 stabilizing agent of the series and was thereby selected for further analysis (Fig. 4).

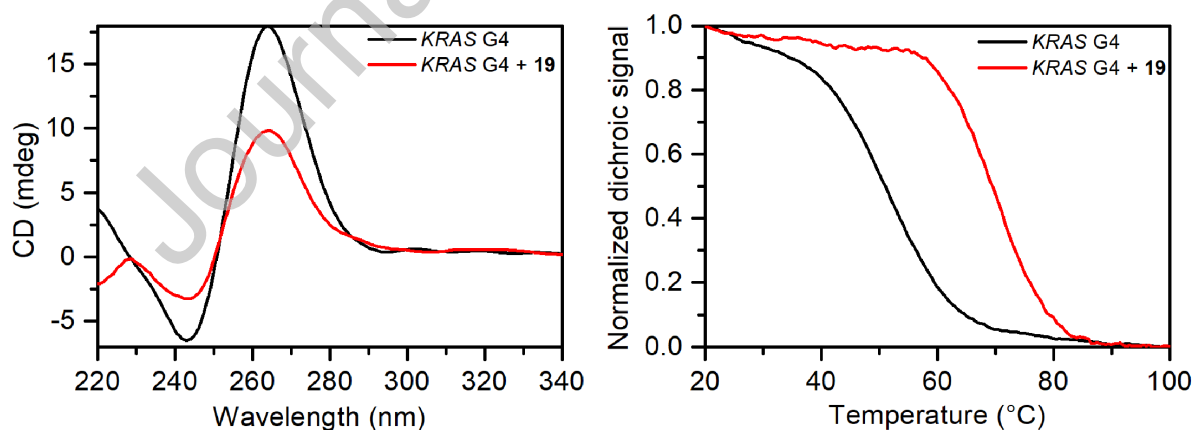


Fig 4. CD spectra (left panel) and thermal melting profiles (right panel) of *KRAS* G4 without (black line) and with (red line) **19**.

Fluorescence titration experiments were thus performed for gaining information on the binding affinity and stoichiometry of the interaction between *KRAS* G4 and **19** (Fig. 5) (Giancola and Pagano, 2013; Pagano et al., 2012). Results of fluorescence analysis showed a stoichiometry ratio of 1:1 *KRAS* G4/**19** and a binding constant (K_b) of $7.2 \pm 0.4 \cdot 10^6 \text{ M}^{-1}$. In order to strengthen the CD results, fluorescence experiments were also performed with *KIT* G4 (Fig. S13), revealing an interaction of 1:1 *KIT* G4/**19** with $K_b = 2.3 \pm 0.5 \cdot 10^6 \text{ M}^{-1}$, which is threefold lower compared to that of *KRAS* G4.

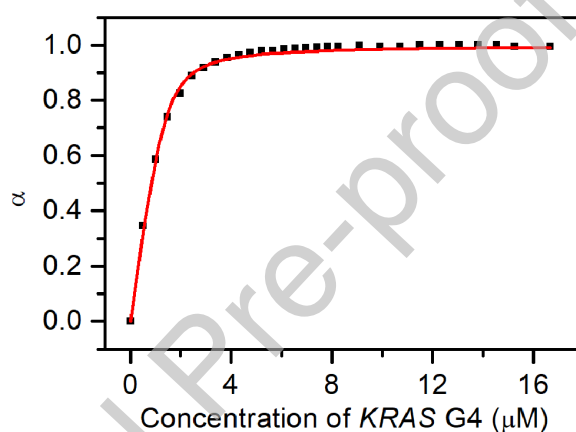


Fig. 5. Fluorescence titration of **19** with *KRAS* G4.

To investigate the behavior of the *KRAS* G4/**19** complex upon addition of different amounts of **19**, a non-denaturing gel electrophoresis (PAGE) experiment was performed (Fig. S14). In fact, *KRAS* G4 moves as a single band in the gel, thus suggesting the absence of high-order DNA structures. The addition of **19** to the *KRAS* G4 did not affect the G4 mobility at all investigated ratios, in agreement with the stoichiometry revealed by the fluorescence assay.

3.5 Computational Studies. In order to investigate at an atomic level the binding mode of the newly synthesized derivatives to *KRAS* G4, molecular modeling studies were carried out on the most promising compound of the series, **19**. Initially, molecular docking of this molecule was

performed on the whole *KRAS* G4 NMR structure (PDB code: 5I2V) (Kerkour et al., 2017). Docking calculations predicted two similar binding modes, A and B (Fig. S15), in which the ligand stacks at the 3' region of the target DNA to interact with residues G9, G13, and A22. However, the two poses differ in the arrangement of the ligand planar scaffold which is mutually flipped by 180°. The stability and the energetics of these poses were then investigated through more accurate calculations. In particular, to fully take into account the receptor flexibility and the water and ions effects, each of the two docking-predicted **19**/DNA complexes was submitted to 1.5 μ s molecular dynamics (MD) simulations in explicit solvent.

A comparison between the ligand RMSD plot computed for the two MD trajectories showed that only one of the two docking solutions (pose A) evolves in a stable binding conformation over the simulated time scale (Fig. S16). In fact, starting from this pose, in the first half of the MD run the ligand experiences a slight rearrangement to reach a well-defined binding mode, which is conserved throughout the rest of the simulation. In fact, this pose is stabilized by tight interactions with the DNA. Specifically, **19** lies at the G4 3' end where it engages favorable π -stacking with G9, G13 and G20 (Fig. 10). Furthermore, the *N,N*-(diethyl)aminoethyl group can alternatively establish a salt bridge with the DNA phosphate backbone of either A14 (Fig. 6) or A22 (Fig. 6C and S17). At this regard, we report that in MD calculations on pose B this kind of ligand-DNA interaction is conversely much less conserved along the whole simulation time (Fig. S18). It is also interesting to note that **19** can form additional stacking interactions with the terminal A22, which shifts from its initial position to be packed against the ligand aromatic scaffold. Remarkably, these contacts stabilize not only the ligand binding conformation but also the overall *KRAS* G4 architecture. This effect can be appreciated by looking at Fig. S19 where the RMSD plot of the G4 backbone along the MD trajectory is shown.

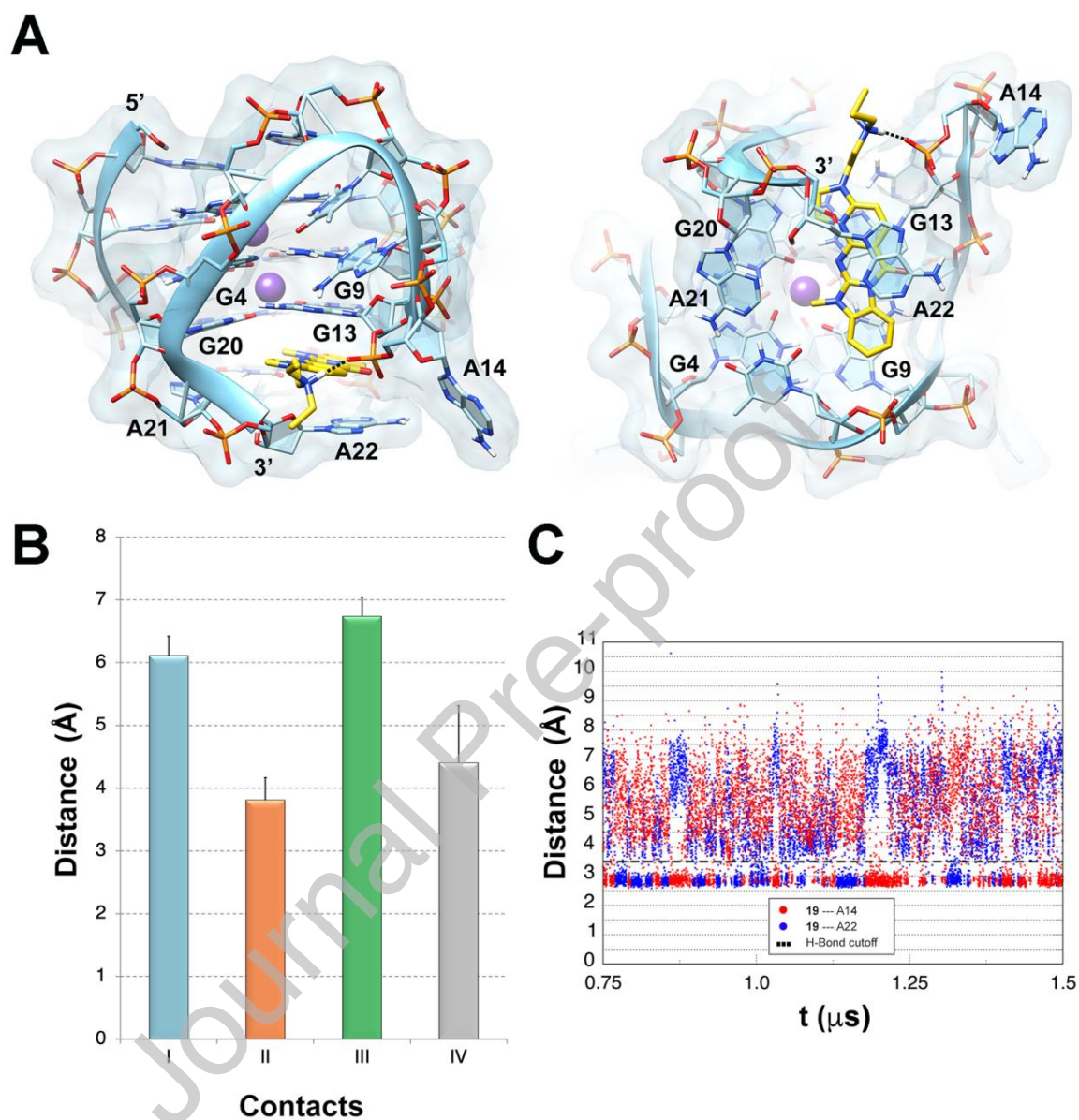


Fig. 6. (A) Front (*left panel*) and bottom (*right panel*) view of the MD predicted binding pose of **19** (yellow sticks) at the NMR structure of the KRAS G4 (PDB code: 5I2V³⁶). DNA is shown as cyan cartoons and transparent surface. Nucleotides are highlighted as sticks; aromatic rings are filled with thin slabs. The color code for the heteroatoms is: blue for nitrogen, red for oxygen. K⁺ ions are depicted as purple spheres. Nonpolar hydrogens are omitted for clarity. Hydrogen bonds

are represented as dashed black lines. (B) Interatomic distances (mean \pm S.D.) representative of the ligand (polycyclic nucleus - center of mass)/DNA residues (aromatic ring centroid) stacking interactions along the second half of the MD calculations on docking pose A: (I) G9, cyan bar; (II) G13, orange bar; (III) G20, green bar; (IV) A22, gray bar. (C) Distance between the ligand diethylamino group (N) and representative A14 and A22 phosphate oxygens along the MD simulations.

3.6 Biological Assays. To verify the biological relevance of our finding, we assayed the capability of **19** to inhibit KRAS expression in tumor cells. To this aim, HCT116 colorectal cancer cells were treated with **19** at 2 μ M concentration, which is the compound IC₅₀ calculated by viability assay (Fig. S20). Also, the effect on KRAS expression was evaluated at both gene and protein level.

As reported in the Fig. 7A, qRT-PCR analysis revealed that treatment of HCT116 colorectal cancer cells with **19** (2 μ M for 24, 48 or 72 h) reduced the mRNA levels of *KRAS* up to 40%, when compared to their untreated counterpart. Subsequently, the effect of **19** on *KRAS* was validated also in terms of protein expression. As evidenced in Fig. 7B, treatment of the cells for 72 h with 2 μ M of **19** determined the reduction of *KRAS* levels of about 30%. Remarkably, in contrast to other G4 ligands, treatment of cells with 2 μ M of **19** for 24 h did not produce any increase in the phosphorylation levels of histone H2AX (γ H2AX, Fig. 7B and S21), a hallmark of DNA double-strand breaks (Thiriet and Hayes, 2005), reinforcing the idea that the selected compound can be selective for the G4 structure present at gene promoter level.

Since *KRAS* is considered a driver oncogene, we also evaluated whether **19** was able to affect the viability of two *KRAS* isogenic tumor cell lines HK2-6 and HKE-3, derived from the

HCT116 cells and carrying the mutated ($KRAS^{G13D/G13D}$) or wild-type ($KRAS^{wt/wt}$) gene alleles, respectively (Del Curatolo et al., 2018; Shirasawa et al., 1993). Briefly, the two cell lines were treated with different concentrations of **19** (ranging from 1 to 10 μM) and the number of viable cells was evaluated by crystal violet assay (Fig. 8). Remarkably, these experiments clearly evidenced that the cytotoxic effect of **19** on the HKE-3 cells ($\text{IC}_{50} > 10 \mu\text{M}$) was lower than that produced on HK2-6 cells ($\text{IC}_{50} = 2.78 \mu\text{M}$). Since the oncogenic potential of KRAS increases in the presence of hotspot mutations (Hobbs et al., 2016), it is possible to conclude that the efficacy of **19** grows together with the activity of KRAS as driver oncogene.

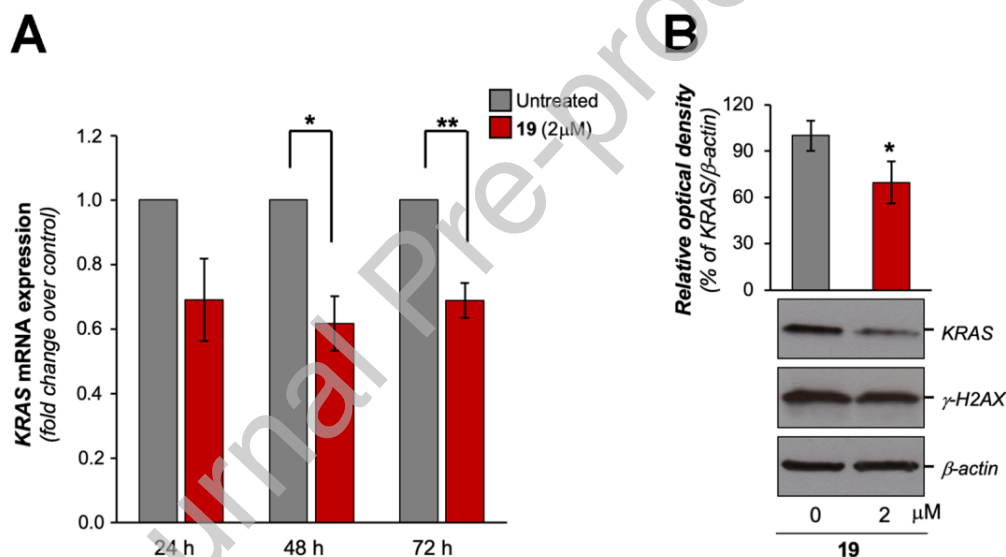


Fig. 7. (A) Gene expression of *KRAS* was evaluated by qPCR in HCT116 cells untreated or treated with 2 μM of **19** for the indicated times (24, 48 and 72 h). Results are expressed as fold change of mRNA levels in treated cells over their controls, after β -actin normalization. Histograms are shown as mean \pm S.D. (* $p \leq 0.05$, ** $p \leq 0.01$; Student's t-test). (B) Protein expression was evaluated by Western Blot (WB) analysis. *Upper panel*, histogram showing the relative optical density of *KRAS* expression evaluated by Image-J quantification tool and

normalized for β -actin. The graph shows the mean \pm S.D. (* $p < 0.05$; Student's t-test). *Lower panel*, representative WB images of KRAS, γ H2AX and β -actin.

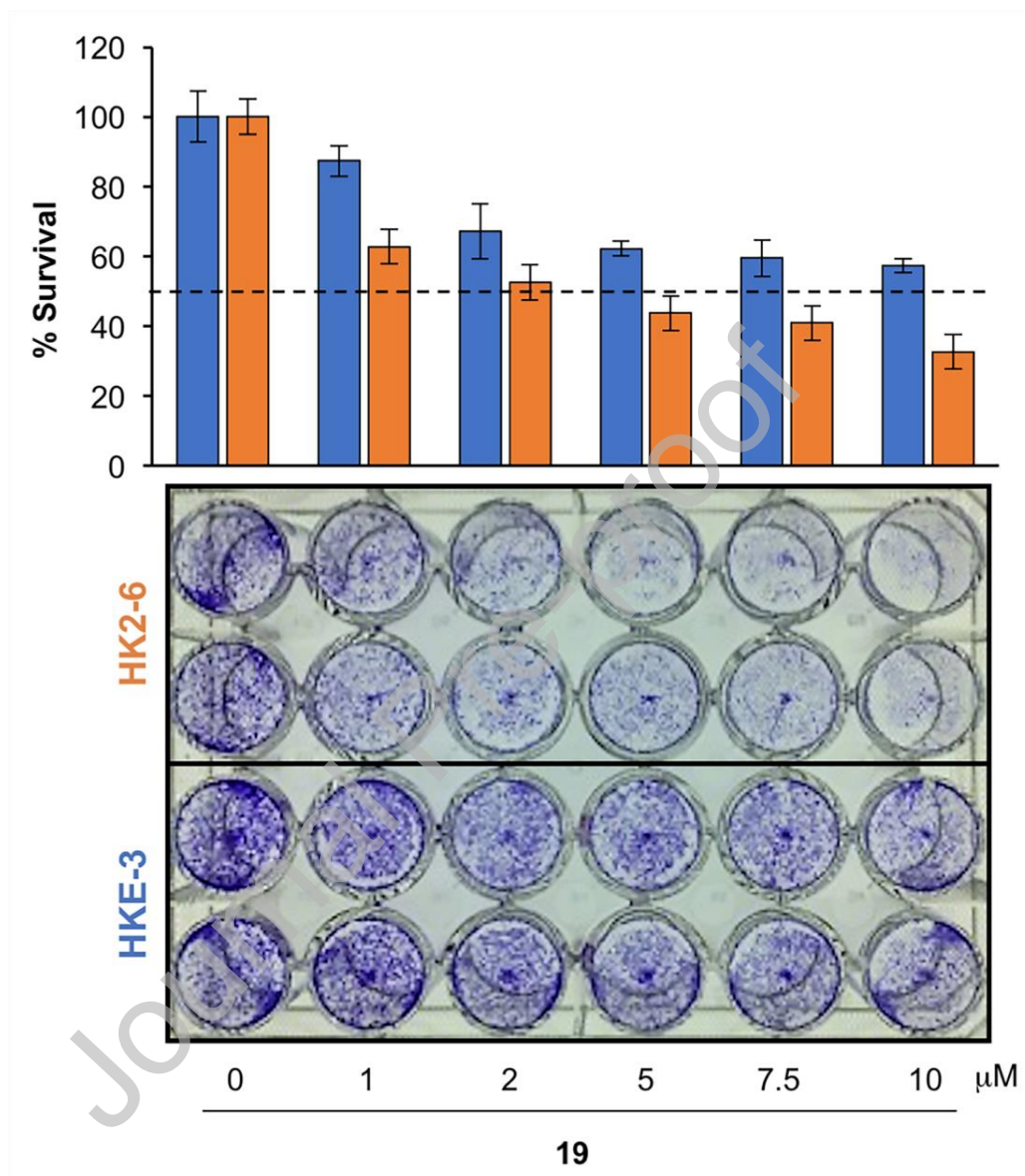


Fig. 8. HK2-6 and HKE-3 cells were treated with compound **19** at the indicated doses for 72 h. Viable cell number was determined by colorimetric crystal violet assay. Histogram shows the mean values \pm S.D..

These data indicate that **19** would represent the prototype of a new class of compounds that, inhibiting the expression of *KRAS* gene, might in principle counteract *KRAS*-mutated tumors that are refractory to treatment with anti-EGFR antibodies (e.g. cetuximab and panitumumab), so far devoid of valid therapeutic treatments (Siravegna et al., 2015).

4. Conclusions

The stabilization of G4 DNA motifs in oncogene promoters by small molecules has emerged in the last years as a promising strategy to control aberrant protein expression in cancer cells (Balasubramanian et al., 2011). Among the druggable oncogenes is *KRAS* which codifies for the homonymous protein and is mutated and overexpressed in a high percentage of tumors (Cogoi and Xodo, 2006; Cox et al., 2014). Here a VS campaign led to the discovery of new chemotypes able to recognize and stabilize a G4 from the *KRAS* P1 promoter. The chemical optimization of the identified molecules resulted in a set of derivatives which were extensively characterized for their G4 stabilizing properties. Particularly one of these analogues, namely **19**, showed a high affinity for the *KRAS* G4 with remarkable selectivity against duplex DNA. Subsequent fluorescence titration experiments on the *KRAS* G4/**19** complex showed a 1:1 stoichiometry ratio and a ligand/DNA binding constant of about $7.2 \cdot 10^6 \text{ M}^{-1}$. Molecular dynamics simulations studies provided not only structural insights into the binding mode of **19** to *KRAS* G4 but also the molecular basis for the stabilization of the target DNA by this compound. Finally, biological assays demonstrated that **19** exerts cytotoxic effects, at low micromolar concentration, in tumor cells expressing constitutively active forms of mutated *KRAS*. In conclusion, our data indicate that **19** can represent the prototype of a novel class of antitumoral drugs able to inhibit the expression of the *KRAS* driver oncogene, which has long been considered undruggable. In this

perspective, the development of a new class of anti-KRAS molecules would represent an important curative opportunity for a subclass of patients for whom effective therapies are still missing (Cox et al., 2014).

Acknowledgements

This research was supported by University of Naples Federico II - “Finanziamento della Ricerca di Ateneo 2016” (prot. n. 16505 to C.G. and F.S.D.L.), and University of Pisa (PRA Project, PRA_2018_20). F.S.D.L. and L.M. and gratefully acknowledge the support by MIUR-PRIN 2015 (Grant FCHJ8E) and MIUR-PRIN 2017 (Grant PHRC8X). C.G., L.M. and F.S.D.L. also acknowledge funding by Regione Campania-POR Campania FESR 2014/2020 (Project N. B61G18000470007). G.C. also acknowledge funding from Italian Association for Cancer Research (AIRC) under IG 2019 (Project ID 23198). Also the work in A.B.’s laboratory has been financially supported by AIRC (Project ID 21579). L.P. and P.Z. are recipients of a fellowship from the Italian Foundation for Cancer Research (FIRC) and the Umberto Veronesi Foundation (FUV), respectively.

Appendix. Supplementary Materials

References

- Alzeer, J., Vummidi, B.R., Roth, P.J.C., Luedtke, N.W., 2009. Guanidinium-modified phthalocyanines as high-affinity G-quadruplex fluorescent probes and transcriptional regulators. *Angew. Chemie - Int. Ed.* <https://doi.org/10.1002/anie.200903685>
- Amato, J., Iaccarino, N., Pagano, B., Morigi, R., Locatelli, A., Leoni, A., Rambaldi, M., Zizza, P., Biroccio, A., Novellino, E., Randazzo, A., 2014a. Bis-indole derivatives with antitumor activity turn out to be specific ligands of human telomeric G-quadruplex. *Front. Chem.*

<https://doi.org/10.3389/fchem.2014.00054>

- Amato, J., Iaccarino, N., Randazzo, A., Novellino, E., Pagano, B., 2014b. Noncanonical DNA secondary structures as drug targets: The prospect of the i-motif. *ChemMedChem*. <https://doi.org/10.1002/cmdc.201402153>
- Bacolla, A., Wells, R.D., 2009. Non-B DNA conformations as determinants of mutagenesis and human disease. *Mol. Carcinog.* <https://doi.org/10.1002/mc.20507>
- Balasubramanian, S., Hurley, L.H., Neidle, S., 2011. Targeting G-quadruplexes in gene promoters: A novel anticancer strategy? *Nat. Rev. Drug Discov.* <https://doi.org/10.1038/nrd3428>
- Banks, J.L., Beard, H.S., Cao, Y., Cho, A.E., Damm, W., Farid, R., Felts, A.K., Halgren, T.A., Mainz, D.T., Maple, J.R., Murphy, R., Philipp, D.M., Repasky, M.P., Zhang, L.Y., Berne, B.J., Friesner, R.A., Gallicchio, E., Levy, R.M., 2005. Integrated Modeling Program, Applied Chemical Theory (IMPACT). *J. Comput. Chem.* <https://doi.org/10.1002/jcc.20292>
- Bayly, C.I., Cieplak, P., Cornell, W.D., Kollman, P.A., 1993. A well-behaved electrostatic potential based method using charge restraints for deriving atomic charges: The RESP model. *J. Phys. Chem.* <https://doi.org/10.1021/j100142a004>
- Biroccio, A., Amodei, S., Antonelli, A., Benassi, B., Zupi, G., 2003. Inhibition of c-Myc oncoprotein limits the growth of human melanoma cells by inducing cellular crisis. *J. Biol. Chem.* <https://doi.org/10.1074/jbc.M304597200>
- Bochman, M.L., Paeschke, K., Zakian, V.A., 2012. DNA secondary structures: Stability and function of G-quadruplex structures. *Nat. Rev. Genet.* <https://doi.org/10.1038/nrg3296>
- Boschi, E., Davis, S., Taylor, S., Butterworth, A., Chirayath, L.A., Purohit, V., Siegel, L.K., Buenaventura, J., Sheriff, A.H., Jin, R., Sheardy, R., Yatsunyk, L.A., Azam, M., 2016. Interaction of a cationic porphyrin and its metal derivatives with G-quadruplex DNA. *J. Phys. Chem. B.* <https://doi.org/10.1021/acs.jpcc.6b09827>
- Calabrese, D.R., Zlotkowski, K., Alden, S., Hewitt, W.M., Connelly, C.M., Wilson, R.M., Gaikwad, S., Chen, L., Guha, R., Thomas, C.J., Mock, B.A., Schneekloth, J.S., 2018. Characterization of clinically used oral antiseptics as quadruplex-binding ligands. *Nucleic Acids Res.* <https://doi.org/10.1093/nar/gky084>
- Cantor, C.R., Warshaw, M.M., Shapiro, H., 1970. Oligonucleotide interactions. III. Circular dichroism studies of the conformation of deoxyoligonucleolides. *Biopolymers.* <https://doi.org/10.1002/bip.1970.360090909>
- Caroti, P., Ceccotti, C., Da Settimo, A., Palla, F., Primofiore, G., 1987. ChemInform Abstract: Synthesis of 5,11-Dihydro-5-oxopyrido(2',3':4,5)pyrimido(1,2-a)benzimidazoles as Potential Antitumor Agents. *ChemInform.* <https://doi.org/10.1002/chin.198744221>
- Carvalho, J., Pereira, E., Marquevielle, J., Campello, M.P.C., Mergny, J.L., Paulo, A., Salgado, G.F., Queiroz, J.A., Cruz, C., 2018. Fluorescent light-up acridine orange derivatives bind and stabilize KRAS-22RT G-quadruplex. *Biochimie.*

<https://doi.org/10.1016/j.biochi.2017.11.004>

- Castillo-González, D., Mergny, J.L., De Rache, A., Pérez-Machado, G., Cabrera-Pérez, M.A., Nicolotti, O., Introcaso, A., Mangiatordi, G.F., Guédin, A., Bourdoncle, A., Garrigues, T., Pallardó, F., Cordeiro, M.N.D.S., Paz-Y-Miño, C., Tejera, E., Borges, F., Cruz-Montegudo, M., 2015. Harmonization of QSAR Best Practices and Molecular Docking Provides an Efficient Virtual Screening Tool for Discovering New G-Quadruplex Ligands. *J. Chem. Inf. Model.* <https://doi.org/10.1021/acs.jcim.5b00415>
- Caterino, M., D'Aria, F., Kustov, A. V., Belykh, D. V., Khudyaeva, I.S., Starseva, O.M., Berezin, D.B., Pylina, Y.I., Usacheva, T., Amato, J., Giancola, C., 2020. Selective binding of a bioactive porphyrin-based photosensitizer to the G-quadruplex from the KRAS oncogene promoter. *Int. J. Biol. Macromol.* <https://doi.org/10.1016/j.ijbiomac.2019.12.152>
- Cogoi, S., Paramasivam, M., Spolaore, B., Xodo, L.E., 2008. Structural polymorphism within a regulatory element of the human KRAS promoter: Formation of G4-DNA recognized by nuclear proteins. *Nucleic Acids Res.* <https://doi.org/10.1093/nar/gkn120>
- Cogoi, S., Quadrioglio, F., Xodo, L.E., 2004. G-rich Oligonucleotide Inhibits the Binding of a Nuclear Protein to the Ki-ras Promoter and Strongly Reduces Cell Growth in Human Carcinoma Pancreatic Cells. *Biochemistry.* <https://doi.org/10.1021/bi035754f>
- Cogoi, S., Xodo, L.E., 2016. G4 DNA in ras genes and its potential in cancer therapy. *Biochim. Biophys. Acta - Gene Regul. Mech.* <https://doi.org/10.1016/j.bbagr.2016.02.002>
- Cogoi, S., Xodo, L.E., 2006. G-quadruplex formation within the promoter of the KRAS proto-oncogene and its effect on transcription. *Nucleic Acids Res.* <https://doi.org/10.1093/nar/gkl286>
- Cogoi, S., Zorzet, S., Rapozzi, V., Géci, I., Pedersen, E.B., Xodo, L.E., 2013. MAZ-binding G4-decoy with locked nucleic acid and twisted intercalating nucleic acid modifications suppresses KRAS in pancreatic cancer cells and delays tumor growth in mice. *Nucleic Acids Res.* <https://doi.org/10.1093/nar/gkt127>
- Cox, A.D., Fesik, S.W., Kimmelman, A.C., Luo, J., Der, C.J., 2014. Drugging the undruggable RAS: Mission Possible? *Nat. Rev. Drug Discov.* <https://doi.org/10.1038/nrd4389>
- Cummaro, A., Fotticchia, I., Franceschin, M., Giancola, C., Petraccone, L., 2011. Binding properties of human telomeric quadruplex multimers: A new route for drug design. *Biochimie.* <https://doi.org/10.1016/j.biochi.2011.04.005>
- Da Costa, K.S., Galúcio, J.M., Da Costa, C.H.S., Santana, A.R., Dos Santos Carvalho, V., Do Nascimento, L.D., Lima E Lima, A.H., Neves Cruz, J., Alves, C.N., Lameira, J., 2019. Exploring the Potentiality of Natural Products from Essential Oils as Inhibitors of Odorant-Binding Proteins: A Structure- And Ligand-Based Virtual Screening Approach to Find Novel Mosquito Repellents. *ACS Omega.* <https://doi.org/10.1021/acsomega.9b03157>
- Da Settimo, A., Da Settimo, F., Marini, A.M., Primofiore, G., Salerno, S., Viola, G., Dalla Via, L., Marciani Magno, S., 1998. Synthesis, DNA binding and in vitro antiproliferative activity

of purinoquinazoline, pyridopyrimidopurine and pyridopyrimidobenzimidazole derivatives as potential antitumor agents. *Eur. J. Med. Chem.* [https://doi.org/10.1016/S0223-5234\(98\)80027-5](https://doi.org/10.1016/S0223-5234(98)80027-5)

Da Settimo, A., Primofiore, G., Da Settimo, F., Marini, A.M., Taliani, S., Salerno, S., Dalla Via, L., 2003. Synthesis of Pyrimido[1,2-a]benzimidazol-4(10H)-one Derivatives and Evaluation of their Interactions with DNA. *J. Heterocycl. Chem.* <https://doi.org/10.1002/jhet.5570400620>

Dai, J., Chen, D., Jones, R.A., Hurley, L.H., Yang, D., 2006a. NMR solution structure of the major G-quadruplex structure formed in the human BCL2 promoter region. *Nucleic Acids Res.* <https://doi.org/10.1093/nar/gkl610>

Dai, J., Dexheimer, T.S., Chen, D., Carver, M., Ambrus, A., Jones, R.A., Yang, D., 2006b. An intramolecular G-quadruplex structure with mixed parallel/antiparallel G-strands formed in the human BCL-2 promoter region in solution. *J. Am. Chem. Soc.* <https://doi.org/10.1021/ja055636a>

Dalla Via, L., Gia, O., Marciani Magno, S., Da Settimo, A., Marini, A.M., Primofiore, G., Da Settimo, F., Salerno, S., 2001. Synthesis, in vitro antiproliferative activity and DNA-interaction of benzimidazoquinazoline derivatives as potential anti-tumor agents. *Farmaco.* [https://doi.org/10.1016/S0014-827X\(01\)01079-5](https://doi.org/10.1016/S0014-827X(01)01079-5)

Darden, T., York, D., Pedersen, L., 1993. Particle mesh Ewald: An $N \cdot \log(N)$ method for Ewald sums in large systems. *J. Chem. Phys.* <https://doi.org/10.1063/1.464397>

Del Curatolo, A., Conciatori, F., Cesta Incani, U., Bazzichetto, C., Falcone, I., Corbo, V., D'Agosto, S., Eramo, A., Sette, G., Sperduti, I., De Luca, T., Marabese, M., Shirasawa, S., De Maria, R., Scarpa, A., Broggin, M., Del Bufalo, D., Cognetti, F., Milella, M., Ciuffreda, L., 2018. Therapeutic potential of combined BRAF/MEK blockade in BRAF-wild type preclinical tumor models. *J. Exp. Clin. Cancer Res.* <https://doi.org/10.1186/s13046-018-0820-5>

Di Leva, F.S., Novellino, E., Cavalli, A., Parrinello, M., Limongelli, V., 2014. Mechanistic insight into ligand binding to G-quadruplex DNA. *Nucleic Acids Res.* <https://doi.org/10.1093/nar/gku247>

Di Leva, F.S., Zizza, P., Cingolani, C., D'Angelo, C., Pagano, B., Amato, J., Salvati, E., Sissi, C., Pinato, O., Marinelli, L., Cavalli, A., Cosconati, S., Novellino, E., Randazzo, A., Biroccio, A., 2013. Exploring the chemical space of G-quadruplex binders: Discovery of a novel chemotype targeting the human telomeric sequence. *J. Med. Chem.* <https://doi.org/10.1021/jm401185b>

Downward, J., 2003. Targeting RAS signalling pathways in cancer therapy. *Nat. Rev. Cancer.* <https://doi.org/10.1038/nrc969>

Feller, S.E., Zhang, Y., Pastor, R.W., Brooks, B.R., 1995. Constant pressure molecular dynamics simulation: The Langevin piston method. *J. Chem. Phys.* <https://doi.org/10.1063/1.470648>

- Fernando, H., Reszka, A.P., Huppert, J., Ladame, S., Rankin, S., Venkitaraman, A.R., Neidle, S., Balasubramanian, S., 2006. A conserved quadruplex motif located in a transcription activation site of the human c-kit oncogene. *Biochemistry*. <https://doi.org/10.1021/bi0601510>
- Franceschin, M., Rizzo, A., Casagrande, V., Salvati, E., Alvino, A., Altieri, A., Ciammaichella, A., Iachettini, S., Leonetti, C., Ortaggi, G., Porru, M., Bianco, A., Biroccio, A., 2012. Aromatic Core Extension in the Series of N-Cyclic Bay-Substituted Perylene G-Quadruplex Ligands: Increased Telomere Damage, Antitumor Activity, and Strong Selectivity for Neoplastic over Healthy Cells. *ChemMedChem*. <https://doi.org/10.1002/cmdc.201200348>
- Friesner, R.A., Banks, J.L., Murphy, R.B., Halgren, T.A., Klicic, J.J., Mainz, D.T., Repasky, M.P., Knoll, E.H., Shelley, M., Perry, J.K., Shaw, D.E., Francis, P., Shenkin, P.S., 2004a. Glide: A New Approach for Rapid, Accurate Docking and Scoring. 1. Method and Assessment of Docking Accuracy. *J. Med. Chem.* <https://doi.org/10.1021/jm0306430>
- Frisch, M.J., Trucks, G.W., Schlegel, H.B., Scuseria, G.E., Robb, M.A., Cheeseman, J.R., Scalmani, G., Barone, V., Mennucci, B., Petersson, G.A., Nakatsuji, H., Caricato, M., Li, X., Hratchian, H.P., Izmaylov, A.F., Bloino, J., Zheng, G., Sonnenberg, J.L., Hada, M., Ehara, M., Toyota, K., Fukuda, R., Hasegawa, J., Ishida, M., Nakajima, T., Honda, Y., Kitao, O., Nakai, H., Vreven, T., Montgomery, J.A., Peralta, J.E., Ogliaro, F., Bearpark, M., Heyd, J.J., Brothers, E., Kudin, K.N., Staroverov, V.N., Kobayashi, R., Normand, J., Raghavachari, K., Rendell, A., Burant, J.C., Iyengar, S.S., Tomasi, J., Cossi, M., Rega, N., Millam, J.M., Klene, M., Knox, J.E., Cross, J.B., Bakken, V., Adamo, C., Jaramillo, J., Gomperts, R., Stratmann, R.E., Yazyev, O., Austin, A.J., Cammi, R., Pomelli, C., Ochterski, J.W., Martin, R.L., Morokuma, K., Zakrzewski, V.G., Voth, G.A., Salvador, P., Dannenberg, J.J., Dapprich, S., Daniels, A.D., Farkas, Foresman, J.B., Ortiz, J. V, Cioslowski, J., Fox, D.J., 2009. Gaussian 09, Revision B.01. Gaussian 09, Revis. B.01, Gaussian, Inc., Wallingford CT.
- Giancola, C., Pagano, B., 2013. Energetics of ligand binding to G-quadruplexes. *Top. Curr. Chem.* <https://doi.org/10.1007/128-2012-347>
- Greenwood, J.R., Calkins, D., Sullivan, A.P., Shelley, J.C., 2010. Towards the comprehensive, rapid, and accurate prediction of the favorable tautomeric states of drug-like molecules in aqueous solution. *J. Comput. Aided. Mol. Des.* <https://doi.org/10.1007/s10822-010-9349-1>
- Grest, G.S., Kremer, K., 1986. Molecular dynamics simulation for polymers in the presence of a heat bath. *Phys. Rev. A.* <https://doi.org/10.1103/PhysRevA.33.3628>
- Haigis, K.M., 2017. KRAS Alleles: The Devil Is in the Detail. *Trends in Cancer.* <https://doi.org/10.1016/j.trecan.2017.08.006>
- Halgren, T.A., Murphy, R.B., Friesner, R.A., Beard, H.S., Frye, L.L., Pollard, W.T., Banks, J.L., 2004. Glide: A New Approach for Rapid, Accurate Docking and Scoring. 2. Enrichment Factors in Database Screening. *J. Med. Chem.* <https://doi.org/10.1021/jm030644s>
- Hobbs, G.A., Der, C.J., Rossman, K.L., 2016. RAS isoforms and mutations in cancer at a glance. *J. Cell Sci.* <https://doi.org/10.1242/jcs.182873>

- Hoffman, E.K., Trusko, S.P., Murphy, M., George, D.L., 1990. An S1 nuclease-sensitive homopurine/homopyrimidine domain in the c-Ki-ras promoter interacts with a nuclear factor. *Proc. Natl. Acad. Sci. U. S. A.* <https://doi.org/10.1073/pnas.87.7.2705>
- Ivani, I., Dans, P.D., Noy, A., Pérez, A., Faustino, I., Hospital, A., Walther, J., Andrio, P., Goñi, R., Balaceanu, A., Portella, G., Battistini, F., Gelpí, J.L., González, C., Vendruscolo, M., Laughton, C.A., Harris, S.A., Case, D.A., Orozco, M., 2015. Parmbsc1: A refined force field for DNA simulations. *Nat. Methods.* <https://doi.org/10.1038/nmeth.3658>
- Janes, M.R., Zhang, J., Li, L.S., Hansen, R., Peters, U., Guo, X., Chen, Y., Babbar, A., Firdaus, S.J., Darjania, L., Feng, J., Chen, J.H., Li, Shuangwei, Li, Shisheng, Long, Y.O., Thach, C., Liu, Yuan, Zariéh, A., Ely, T., Kucharski, J.M., Kessler, L. V., Wu, T., Yu, K., Wang, Y., Yao, Y., Deng, X., Zarrinkar, P.P., Brehmer, D., Dhanak, D., Lorenzi, M. V., Hu-Lowe, D., Patricelli, M.P., Ren, P., Liu, Yi, 2018. Targeting KRAS Mutant Cancers with a Covalent G12C-Specific Inhibitor. *Cell.* <https://doi.org/10.1016/j.cell.2018.01.006>
- Jordano, J., Perucho, M., 1986. Chromatin structure of the promoter region of the human c-K-ras gene. *Nucleic Acids Res.* 14, 7361–7378. <https://doi.org/10.1093/nar/14.18.7361>
- Jorgensen, W.L., Chandrasekhar, J., Madura, J.D., Impey, R.W., Klein, M.L., 1983. Comparison of simple potential functions for simulating liquid water. *J. Chem. Phys.* <https://doi.org/10.1063/1.445869>
- Kang, R., Xie, Y., Zhang, Q., Hou, W., Jiang, Q., Zhu, S., Liu, J., Zeng, D., Wang, H., Bartlett, D.L., Billiar, T.R., Zeh, H.J., Lotze, M.T., Tang, D., 2017. Intracellular HMGB1 as a novel tumor suppressor of pancreatic cancer. *Cell Res.* <https://doi.org/10.1038/cr.2017.51>
- Kerkour, A., Marquevielle, J., Ivashchenko, S., Yatsunyk, L.A., Mergny, J.L., Salgado, G.F., 2017. High-resolution three-dimensional NMR structure of the KRAS proto-oncogene promoter reveals key features of a G-quadruplex involved in transcriptional regulation. *J. Biol. Chem.* <https://doi.org/10.1074/jbc.M117.781906>
- La Pietra, V., Sartini, S., Botta, L., Antonelli, A., Ferrari, S.M., Fallahi, P., Moriconi, A., Coviello, V., Quattrini, L., Ke, Y.Y., Hsing-Pang, H., Da Settimo, F., Novellino, E., La Motta, C., Marinelli, L., 2018. Challenging clinically unresponsive medullary thyroid cancer: Discovery and pharmacological activity of novel RET inhibitors. *Eur. J. Med. Chem.* <https://doi.org/10.1016/j.ejmech.2018.02.080>
- Lavrado, J., Borralho, P.M., Ohnmacht, S.A., Castro, R.E., Rodrigues, C.M.P., Moreira, R., Dos Santos, D.J.V.A., Neidle, S., Paulo, A., 2013. Synthesis, G-quadruplex stabilisation, docking studies, and effect on cancer cells of indolo[3,2-b]quinolines with one, two, or three basic side chains. *ChemMedChem.* <https://doi.org/10.1002/cmdc.201300288>
- Lavrado, J., Brito, H., Borralho, P.M., Ohnmacht, S.A., Kim, N.S., Leitão, C., Pisco, S., Gunaratnam, M., Rodrigues, C.M.P., Moreira, R., Neidle, S., Paulo, A., 2015. KRAS oncogene repression in colon cancer cell lines by G-quadruplex binding indolo[3,2-c]quinolines. *Sci. Rep.* <https://doi.org/10.1038/srep09696>
- Lito, P., Solomon, M., Li, L.S., Hansen, R., Rosen, N., 2016. Cancer therapeutics: Allele-specific

- inhibitors inactivate mutant KRAS G12C by a trapping mechanism. *Science* (80-.). <https://doi.org/10.1126/science.aad6204>
- Madhavi Sastry, G., Adzhigirey, M., Day, T., Annabhimoju, R., Sherman, W., 2013. Protein and ligand preparation: Parameters, protocols, and influence on virtual screening enrichments. *J. Comput. Aided. Mol. Des.* <https://doi.org/10.1007/s10822-013-9644-8>
- Martyna, G.J., Tobias, D.J., Klein, M.L., 1994. Constant pressure molecular dynamics algorithms. *J. Chem. Phys.* <https://doi.org/10.1063/1.467468>
- McCormick, F., 2018. Targeting KRAS Directly. *Annu. Rev. Cancer Biol.* <https://doi.org/10.1146/annurev-cancerbio-050216-122010>
- McCormick, F., 2016. K-Ras protein as a drug target. *J. Mol. Med.* <https://doi.org/10.1007/s00109-016-1382-7>
- Miglietta, G., Cogoi, S., Marinello, J., Capranico, G., Tikhomirov, A.S., Shchekotikhin, A., Xodo, L.E., 2017. RNA G-Quadruplexes in Kirsten Ras (KRAS) Oncogene as Targets for Small Molecules Inhibiting Translation. *J. Med. Chem.* <https://doi.org/10.1021/acs.jmedchem.7b00622>
- Miyamoto, S., Kollman, P.A., 1992. Settle: An analytical version of the SHAKE and RATTLE algorithm for rigid water models. *J. Comput. Chem.* <https://doi.org/10.1002/jcc.540130805>
- Monchaud, D., Teulade-Fichou, M.P., 2008. A hitchhiker's guide to G-quadruplex ligands. *Org. Biomol. Chem.* <https://doi.org/10.1039/b714772b>
- Naidu, S., Shi, L., Magee, P., Middleton, J.D., Laganá, A., Sahoo, S., Leong, H.S., Galvin, M., Frese, K., Dive, C., Guzzardo, V., Fassan, M., Garofalo, M., 2017. PDGFR-modulated miR-23b cluster and miR-125a-5p suppress lung tumorigenesis by targeting multiple components of KRAS and NF- κ B pathways. *Sci. Rep.* <https://doi.org/10.1038/s41598-017-14843-6>
- Oliviero, G., D'Errico, S., Borbone, N., Amato, J., Piccialli, V., Varra, M., Piccialli, G., Mayol, L., 2010. A solid-phase approach to the synthesis of N-1-alkyl analogues of cyclic inosine-diphosphate-ribose (ciDPR). *Tetrahedron.* <https://doi.org/10.1016/j.tet.2010.01.013>
- Ostrem, J.M., Peters, U., Sos, M.L., Wells, J.A., Shokat, K.M., 2013. K-Ras(G12C) inhibitors allosterically control GTP affinity and effector interactions. *Nature.* <https://doi.org/10.1038/nature12796>
- Pagano, B., Cosconati, S., Gabelica, V., Petraccone, L., De Tito, S., Marinelli, L., La Pietra, V., Saverio di Leva, F., Lauri, I., Trotta, R., Novellino, E., Giancola, C., Randazzo, A., 2012. State-of-the-Art Methodologies for the Discovery and Characterization of DNA G-Quadruplex Binders. *Curr. Pharm. Des.* <https://doi.org/10.2174/138161212799958332>
- Parenty, A.D.C., Smith, L. V., Cronin, L., 2005. An unusual substitution reaction directed by an intramolecular re-arrangement. *Tetrahedron.* <https://doi.org/10.1016/j.tet.2005.06.074>
- Parenty, A.D.C., Song, Y.F., Richmond, C.J., Cronin, L., 2007. A general and efficient five-step one-pot procedure leading to nitrogen-bridgehead heterocycles containing an imidazole

ring. *Org. Lett.* <https://doi.org/10.1021/ol070263z>

- Patricelli, M.P., Janes, M.R., Li, L.S., Hansen, R., Peters, U., Kessler, L. V., Chen, Y., Kucharski, J.M., Feng, J., Ely, T., Chen, J.H., Firdaus, S.J., Babbar, A., Ren, P., Liu, Y., 2016. Selective inhibition of oncogenic KRAS output with small molecules targeting the inactive state. *Cancer Discov.* <https://doi.org/10.1158/2159-8290.CD-15-1105>
- Pattanayak, R., Barua, A., Das, A., Chatterjee, T., Pathak, A., Choudhury, P., Sen, S., Saha, P., Bhattacharyya, M., 2018. Porphyrins to restrict progression of pancreatic cancer by stabilizing KRAS G-quadruplex: In silico, in vitro and in vivo validation of anticancer strategy. *Eur. J. Pharm. Sci.* <https://doi.org/10.1016/j.ejps.2018.09.011>
- Phillips, J.C., Braun, R., Wang, W., Gumbart, J., Tajkhorshid, E., Villa, E., Chipot, C., Skeel, R.D., Kalé, L., Schulten, K., 2005. Scalable molecular dynamics with NAMD. *J. Comput. Chem.* <https://doi.org/10.1002/jcc.20289>
- Pinto, V. de S., Araújo, J.S.C., Silva, R.C., da Costa, G. V., Cruz, J.N., Neto, M.F.D.A., Campos, J.M., Santos, C.B.R., Leite, F.H.A., Junior, M.C.S., 2019. In silico study to identify new antituberculosis molecules from natural sources by hierarchical virtual screening and molecular dynamics simulations. *Pharmaceuticals.* <https://doi.org/10.3390/ph12010036>
- Rankin, S., Reszka, A.P., Huppert, J., Zloh, M., Parkinson, G.N., Todd, A.K., Ladame, S., Balasubramanian, S., Neidle, S., 2005. Putative DNA quadruplex formation within the human c-kit oncogene. *J. Am. Chem. Soc.* <https://doi.org/10.1021/ja050823u>
- Ryckaert, J.P., Ciccotti, G., Berendsen, H.J.C., 1977. Numerical integration of the cartesian equations of motion of a system with constraints: molecular dynamics of n-alkanes. *J. Comput. Phys.* [https://doi.org/10.1016/0021-9991\(77\)90098-5](https://doi.org/10.1016/0021-9991(77)90098-5)
- Shelley, J.C., Cholleti, A., Frye, L.L., Greenwood, J.R., Timlin, M.R., Uchimaya, M., 2007. Epik: A software program for pKa prediction and protonation state generation for drug-like molecules. *J. Comput. Aided. Mol. Des.* <https://doi.org/10.1007/s10822-007-9133-z>
- Shirasawa, S., Furuse, M., Yokoyama, N., Sasazuki, T., 1993. Altered growth of human colon cancer cell lines disrupted at activated Ki-ras. *Science* (80-). <https://doi.org/10.1126/science.8465203>
- Siddiqui-Jain, A., Grand, C.L., Bearss, D.J., Hurley, L.H., 2002. Direct evidence for a G-quadruplex in a promoter region and its targeting with a small molecule to repress c-MYC transcription. *Proc. Natl. Acad. Sci. U. S. A.* <https://doi.org/10.1073/pnas.182256799>
- Simonsson, T., Pecinka, P., Kubista, M., 1998. DNA tetraplex formation in the control region of c-myc. *Nucleic Acids Res.* <https://doi.org/10.1093/nar/26.5.1167>
- Siravegna, G., Mussolin, B., Buscarino, M., Corti, G., Cassingena, A., Crisafulli, G., Ponzetti, A., Cremolini, C., Amatu, A., Lauricella, C., Lamba, S., Hobor, S., Avallone, A., Valtorta, E., Rospo, G., Medico, E., Motta, V., Antoniotti, C., Tatangelo, F., Bellosillo, B., Veronese, S., Budillon, A., Montagut, C., Racca, P., Marsoni, S., Falcone, A., Corcoran, R.B., Di Nicolantonio, F., Loupakis, F., Siena, S., Sartore-Bianchi, A., Bardelli, A., 2015. Clonal

- evolution and resistance to EGFR blockade in the blood of colorectal cancer patients. *Nat. Med.* <https://doi.org/10.1038/nm.3870>
- Stephen, A.G., Esposito, D., Bagni, R.G., McCormick, F., 2014. Dragging ras back in the ring. *Cancer Cell.* <https://doi.org/10.1016/j.ccr.2014.02.017>
- Sun, D., Guo, K., Rusche, J.J., Hurley, L.H., 2005. Facilitation of a structural transition in the polypurine/polypyrimidine tract within the proximal promoter region of the human VEGF gene by the presence of potassium and G-quadruplex-interactive agents. *Nucleic Acids Res.* <https://doi.org/10.1093/nar/gki917>
- Thiriet, C., Hayes, J.J., 2005. Chromatin in need of a fix: Phosphorylation of H2AX connects chromatin to DNA repair. *Mol. Cell.* <https://doi.org/10.1016/j.molcel.2005.05.008>
- Wang, J., Cieplak, P., Kollman, P.A., 2000. How Well Does a Restrained Electrostatic Potential (RESP) Model Perform in Calculating Conformational Energies of Organic and Biological Molecules? *J. Comput. Chem.* [https://doi.org/10.1002/1096-987X\(200009\)21:12<1049::AID-JCC3>3.0.CO;2-F](https://doi.org/10.1002/1096-987X(200009)21:12<1049::AID-JCC3>3.0.CO;2-F)
- Wang, J., Wang, W., Kollman, P.A., Case, D.A., 2006. Automatic atom type and bond type perception in molecular mechanical calculations. *J. Mol. Graph. Model.* <https://doi.org/10.1016/j.jmgm.2005.12.005>
- Wang, J., Wolf, R.M., Caldwell, J.W., Kollman, P.A., Case, D.A., 2004. Development and testing of a general Amber force field. *J. Comput. Chem.* <https://doi.org/10.1002/jcc.20035>
- Zhang, D.H., Fujimoto, T., Saxena, S., Yu, H.Q., Miyoshi, D., Sugimoto, N., 2010. Monomorphic RNA G-quadruplex and polymorphic DNA G-quadruplex structures responding to cellular environmental factors. *Biochemistry.* <https://doi.org/10.1021/bi1002822>
- Zhao, J., Bacolla, A., Wang, G., Vasquez, K.M., 2010. Non-B DNA structure-induced genetic instability and evolution. *Cell. Mol. Life Sci.* <https://doi.org/10.1007/s00018-009-0131-2>
- Zizza, P., Dinami, R., Porru, M., Cingolani, C., Salvati, E., Rizzo, A., D'Angelo, C., Petti, E., Amoreo, C.A., Mottolese, M., Sperduti, I., Chambery, A., Russo, R., Ostano, P., Chiorino, G., Blandino, G., Sacconi, A., Cherfils-Vicini, J., Leonetti, C., Gilson, E., Biroccio, A., 2019. TRF2 positively regulates SULF2 expression increasing VEGF - A release and activity in tumor microenvironment. *Nucleic Acids Res.* <https://doi.org/10.1093/nar/gkz041>

Credit Author statement

Federica D’Aria: Physicochemical Studies, Data curation, Validation, Writing - Original draft preparation. **Vincenzo Maria D’Amore:** Computational Studies, Data curation, Validation, Writing- Original draft preparation. **Francesco Saverio Di Leva:** Computational studies, Conceptualization, Supervision, Funding acquisition, Writing - reviewing & editing. **Jussara Amato:** Physicochemical Studies, Supervision. **Marco Caterino:** Physicochemical Studies. **Pasquale Russomanno:** Computational Studies. **Silvia Salerno:** Chemical Synthesis. **Elisabetta Barresi:** Chemical Synthesis. **Marinella De Leo:** Chemical Synthesis. **Anna Maria Marini:** Chemical Synthesis. **Sabrina Taliani:** Chemical Synthesis, Supervision, Funding acquisition. **Federico Da Settimo:** Chemical Synthesis, Supervision. **Gilmar F. Salgado:** Writing - reviewing & editing. **Luca Pompili:** Biological evaluation. **Pasquale Zizza:** Biological evaluation, Data Validation, Writing - Original draft preparation. **Senji Shirasawa:** Biological evaluation. **Ettore Novellino:** Supervision, Funding acquisition. **Annamaria Biroccio:** Biological evaluation, Supervision, Funding acquisition. **Luciana Marinelli:** Computational Studies, Conceptualization, Supervision, Funding acquisition. **Concetta Giancola:** Physicochemical Studies, Conceptualization, Supervision, Funding acquisition, Writing - reviewing & editing.

Graphical abstract

